OAK RIDGE
NATIONAL LABORATORY

MANAGED BY UT-BATTELLE
FOR THE DEPARTMENT OF ENERGY

Note on Graphite Oxidation by Oxygen and Moisture

November 2008

Prepared by
Robert P. Wichner
Oak Ridge National Laboratory

UT–BATTELLE

ORNL-27 (4-00)

Materials Science and Technology Division

Note on Graphite Oxidation by Oxygen and Moisture

Robert P. Wichner [1]
Timothy D. Burchell [2]
Cristian I. Contescu [3]

[1] Consultant, Carbon Materials Technology Group, Materials Science and Technology Division
[2] Leader, Carbon Materials Technology Group, Materials Science and Technology Section
[3] Carbon Materials Technology Group, Materials Science and Technology Division

Date published: November 2008

This page was intentionally left blank

CONTENTS

LIST OF FIGURES

This page was intentionally left blank.

LIST OF TABLES

This page was intentionally left blank.

SUMMARY

The objective of this memo is to review some of the simplified equations of graphite oxidation that may have been better known at the time when there were larger active programs. Toward this end, equations for oxidant distribution and surface oxidation rate are derived for the semi-infinite slab, finite slab, and cylinder under the main assumptions of linearized oxidation kinetics and fully established oxidation profile. The equations are coupled with a general expression for the surface mass transfer. Other assumptions are pointed out which are implied in derivations, but which may easily be overlooked.

These equations, though approximate, are still useful for general purposes, such as identifying the region of zone-1 oxidation in laboratory experiments and ready estimates of oxidation rate. Some examples are given intended mainly as illustration. All results are easily reproducible by spreadsheet calculations.

Re-derivation of these equations has nevertheless brought out some features that may not have been previously noted, at least not obviously. Some of these are as follows.

- The impact of the effective diffusivity (D_{eff}) of oxidant in graphite on the surface oxidation rate and on the oxidant profiles is shown. It is seen that increasing D_{eff} increases the surface oxidation rate and flattens the oxidant concentration profile, all other parameters equal.

- A short review is presented on the physical interpretation of D_{eff}, including some measured values taken from 40-year old research reports. Variation of D_{eff} with temperature and graphite density is central to proper estimation of oxidation rates in large members.

- The distribution of hydrogen in graphite is derived for the case of oxidation by H_2O. As anticipated, hydrogen concentrations are always higher in the graphite than in the free stream. Approximate equations for hydrogen distribution are given for the slab and the long cylinder.

- A method is presented for determining the time required for achieving equilibration to the quasi-steady oxidation profile. It is shown that the equilibration times are quite short at temperatures of 800 K and above, but increase sharply at lower temperatures.

- The effect of stoichiometry, i.e., the CO to CO_2 product ratio, on concentration distributions and surface oxidation rate is included in the derivations.

- A more complete temperature dependence of the surface oxidation rate is derived than generally given. Usually, a square root temperature dependence is cited for the diffusivity-affected regime. Careful evaluation shows that at least two other factors modify this generalization, one due to the effect of temperature on the mass transfer boundary condition, the other resulting from the conversion of partial pressure to concentration in the kinetics equation.

- An oxidation efficiency parameter is derived for slab and cylinder geometry akin to the catalyst efficiency factor. The parameter approaches unity for uniform oxidation and tends toward zero as surface oxidation is approached at high temperature. The parameter is useful for defining zone-1 experimental conditions.

- A simple relation is shown between the quasi-steady oxidant concentration profile, as derived by equations in this memo, and the burnoff profile.

This page was intentionally left blank.

ABSTRACT

Simplified equations of graphite oxidation are reviewed for semi-infinite slab, finite slab, and cylinder geometries, using the principal assumptions of linearized oxidation kinetics and quasi-steady state oxidation profile. All equations are coupled to a general surface mass transfer boundary condition. The equations include those for oxidant concentration distribution, surface oxidation rate, burnoff profile, and oxidation efficiency. This review also covers some areas that may not be well recognized. The key role of the effective diffusivity is highlighted, with a brief review of measured values. The temperature-dependence of the surface oxidation rate is shown to be more complex than usually shown for the diffusion-affected zone. Assumption of linear kinetics permits ready estimation of equilibration time for development of the quasi-steady burnoff profile. In addition, approximations for the time-steady hydrogen concentration profiles are developed for the case of oxidation by H_2O. All cited methods can be readily evaluated by spreadsheet calculation.

1. INTRODUCTION

After a long hiatus, the interest in graphite oxidation has resumed, but under a somewhat different set of circumstances. Development of computer capability and general transport codes that can resolve time-dependent non-linear equations now free the analysts of time-consuming mathematical compromise. The emphasis should now be on the understanding the phenomena sufficiently well to enable proper application of the codes, and on the acquisition of the necessary input data to run the codes.

Because of the renewed interest, a review of some older concepts may be useful. To this end, equations for oxidant concentration profiles are presented for the semi-infinite slab, finite slab and long cylinder, based on assumptions of quasi-steady state and linearized oxidation kinetics. More complex approaches that attempt to introduce a more complete mechanistic realism, e.g., by accounting for chemical interactions of the various component phases comprising graphite, Knudsen diffusion in micropores, size distribution of porosity, and other factors, have a history of leading to an impractical degree of complexity.

Though this memo is intended as a review, an overall impression emerges of the central importance of a semi-empirical, effective diffusion coefficient as an approach to general solution of graphite oxidation. A method is shown whereby the transient, non-linear, general oxidation equation may be solved in conjunction with the oxidant transport equation (and the hydrogen transport equation for the case of oxidation by H_2O), provided a functional relationship is known between the effective diffusivity and key local properties.

In this report, the quasi-steady state, linearized oxidant transport equations (and the H_2 transport equation for oxidation by H_2O) are coupled to the surface convection boundary condition. Solutions may thus be used to visualize the effects of altering temperature, oxidant concentration (and H_2 concentration), and mass transfer coefficients on oxidant, (and H_2), and graphite density profiles.

The oxidant profiles are integrated to yield the surface oxidation rate, as first presented by Thiele. However, the factors contributing to the surface rate, e.g. stoichiometric constants and temperature, are here more carefully considered than in earlier treatments.

The solutions for the oxidant profiles lead to criteria for establishing Zone-1 conditions in slab and cylinder laboratory specimens, based on "oxidation efficiency factors", as suggested by the analogous "catalyst effective factors".

Some examples of concentration profiles and surface oxidation rates are shown, assuming laminar flow conditions typical of a small laboratory apparatus, and using preliminary values of O_2 and H_2O oxidation kinetics constants. Surface concentration reductions may be seen at the higher temperatures. The surface oxidation rate is derived and its variation with temperature is shown for slab and cylinder geometry.

Additional items covered are the following:

2

(1) A system of equations is presented that expresses the general, space and time dependent graphite oxidation rate, the solution of which is a worthy objective for a large-scale computer program.

(2) The importance of the effective diffusion coefficient (D_{eff}) is cited. A brief survey of D_{eff} data is presented.

(3) The relation of the graphite density profile to the quasi-steady state oxidant concentration profile is developed.

(4) An expression is developed for the time required to establish the quasi-steady state profile. The time is shown to be quite short for O_2 oxidation at 800K and above.

However it should be emphasized that the main purpose of this memo is to review older concepts and present them as a convenient unity. Any additional benefits that may have accrued are more-or-less incidental to the main purpose. Nevertheless, the equations could provide convenient, ready estimates.

2. GENERAL GRAPHITE OXIDATION EQUATION

The general equation for oxidative loss of carbon at vector location $\underline{r}$ in graphite and time t may be written,

$$\partial\rho(\underline{r},t)/\partial t = R_1(\underline{r},t)\,\rho(\underline{r},t) \tag{1}$$

where

ρ graphite molar density, mol/m^3-geom
R_1 kinetic oxidation rate, mol C oxidized/mol C.sec
$\underline{r}$ vector location

R_1 is the diffusion-unaffected oxidation rate obtained from conventional small specimen kinetics equation, evaluated at the local condition $(\underline{r},t)$. It is usually expressed on a per mole (or per kg) basis and must therefore be multiplied by $\rho(\underline{r},t)$ to convert to units of moles carbon loss per m^3-geom.[1] Thus the units of each term are mol-C/m^3-geom•sec. R_1 may refer to either O_2 or H_2O oxidation.

Assuming R_1 can be evaluated from a known kinetic equation, the solution of (1) for the oxidation distribution, $\rho(\underline{r},t)$, requires knowledge of the local oxidant concentration, which depends on all the parameters affecting oxidant distribution, including,

(1) surface oxidant concentration
(2) effective diffusivity of oxidant (D_{eff})
(3) stoichiometry of the oxidation reaction
(4) value of the conversion function, $f(\alpha)$.

A mathematically complex system of equations results that requires simultaneous solution of equation (1) with the oxidant transport equation (and the H_2 transport equation in the case of H_2O oxidation). The equations are non-linear because of the appearance of the graphite density (or porosity, or degree of conversion) in all terms, explicitly as in (1) or implicitly in the dependence of effective diffusivity (D_{eff}) and conversion function, $f(\alpha)$, in the oxidant transport equation.

---

[1] It is necessary to distinguish between m^3-geom, referring to the entire graphite space, and m^3-void, referring only to the void portion of the graphite. The oxidant concentration will be expressed in terms of mol/m^3-void.

3. OXIDANT TRANSPORT EQUATION

The time-dependant O_2 transport equation is obtained by equating the loss of O_2 from a volume element to the sum of losses due to diffusion and oxidation. In general coordinates,

$$\partial(\varepsilon u)/\partial t = -\nabla \bullet [D_{eff} \ \nabla u(\underline{r},t)] - R_1 \rho N_{O2} \tag{2}$$

For notational simplicity, the symbol, u, is used for oxidant concentration in the graphite with units mol/m^3-void. The void fraction, ε, in the time derivative is needed to express the LHS as mol O_2/m^3-geom.sec.[2] Each term is consistently expressed in these units. As a result, the effective diffusivity, D_{eff}, takes the apparently odd dimensionality of m^3-void/m-geom.sec. D_{eff} is included within the divergence operator because it is a function of the void fraction, hence a function of space.

The oxidation rate per unit mass, R_1, is converted to the rate per unit volume by multiplying by the molar density. The loss rate of O_2 is obtained by multiplication by the stoichiometric parameter, N_{H2O}, defined as,

N_{O2} moles of oxidant consumed/mole C oxidized.

For O_2 oxidation its value ranges from unity, for 100% CO_2 product, to 0.5 for production of entirely CO. A similar term, N_{H2O} used for H_2O oxidation will also depend on the local stoichiometry of the reaction. It is entirely possible that N_{O2} (or N_{H2O}) can vary within the graphite depending on the local oxidant concentration.

R_1 for O_2 oxidation is generally expressed as

$$R_1 = K_1 \exp(-H/RT) f(\alpha) (P_{O2})^n \tag{3}$$

The reaction order, n, is often given as 0.8. However oxidation data, with its normal scatter, may also be correlated assuming $n = 1$, as in GDH (1988) for Stackpole 2020 graphite. The GDH gives for Stackpole 2020,

$K_1 = 0.79$ (sec•Pa)$^{-1}$
$H = 1.7 \times 10^5$ J/mol•K
$n = 1$

$f(\alpha)$ is the conversion function, with α defined as the degree of conversion, i.e., the fractional burnoff. $f(\alpha)$ ranges from unity at $\alpha = 0$, to a maximum of about 5 at α of approximately 0.2, thereafter declining to 0 at complete conversion.

The void fraction differs slightly from, α, the degree of conversion:

$$\varepsilon = 1 - \rho/\rho_{theo} \tag{4}$$

---

[2] Hinsson (2006) writes the first term as $\varepsilon \bullet \partial u/\partial t$. However, ε should be within the partial derivative since $\partial \varepsilon/\partial t$ affects the oxidant concentration in the pores when there is spatial variation.

compared with

$$\alpha = 1 - \rho/\rho_\infty \tag{5}$$

where ρ_{theo} is the theoretical graphite density, and ρ_∞ the unoxidized density. In practical terms, the two may be considered equivalent.

4. EFFECTIVE DIFFUSIVITY

4.1 Approximations

Equation (2) presumes that movement of oxidant gas in graphite may be expressed as diffusion along connected porosity using a semi-empirical effective diffusion coefficient, D_{eff}. Since D_{eff} is expected to vary with burnoff (i.e., porosity, density, or degree of conversion), which in general varies in location, it is placed within the divergence operator.

Equation (2) states that diffusion may be expressed as

$$J_i = -D_{eff}\nabla C_i,$$

where C_i is the concentration of species-i, mol/m^3-pores. However, it is well known that multicomponent diffusion cannot, in general, be expressed so simply. For example, Hines and Maddox (1985) write,

$$J_i = -D_{eff}\nabla C_i + C_i\underline{V}$$.

That is, the molar flux of species-i with respect to a fixed reference frame is equal to the sum of an effective diffusion rate, which is relative to a molar average velocity, plus a convection term ($\underline{V}$ is the molar average vector velocity) required to maintain constant pressure in gases diffusing at different rates or changing in volume due to chemical reaction. The convection velocity may be determined in simple cases, but only with a great difficulty for the complex case of multiple diffusing species being added and removed by oxidation with a reactive boundary, and further, in a complex, three dimensional pore geometry.

However, the Fickian form is approached at low concentrations as the molar average velocity approaches zero. The complexities of dealing with diffusion-induced convection in multi-component diffusion are such that the Fickian form is often assumed even when it is technically not applicable, such as for air ingress where the mole fraction of diffusing species approach 0.2. (E.g., see Hinssen et al, 2006).

In addition to molecular diffusion, which has thus far been implied, Knudsen diffusion and surface diffusion may, in principle, contribute to the total rate of transport. Evans et al (1961) show that the three modes of transport may be combined into a single effective diffusivity for a simple binary system. Oxidation is generally more complicated. involving more than two components. More importantly, each transport mode is affected in different ways by temperature, pressure and pore configuration. Therefore, for practical reasons, consideration is limited to molecular diffusion. This is not a severe limitation for graphite oxidation.

Knudsen diffusion is not important for pores diameters above about 0.2 microns at one atmosphere total pressure and smaller diameters at higher pressures. Since the dominant pore size is typically several microns in graphite, Knudsen diffusion is not likely to be an important factor.

Similarly, surface diffusion is not likely to be significant for non-condensing, dilute, oxidant gases at high temperature.

There is a large literature on multi-component diffusion in porous media, much of it summarized by Aris (1975). Examination shows that such theories invariably result in complexities that make them inappropriate for general application. Also they introduce difficult-to-evaluate new parameters, which, at best, require extensive experimentation, especially considering that we are dealing with a range of different graphites and burnoffs. Many theories focus on the specific difficulties associated with combined Knudsen and molecular diffusion, as may be expected for studies of catalyst behavior, where most of these studies originate. Some involve diffusion of condensable species. Even so, none approach the complexity inherent in diffusion in a three-dimensional, time-varying, chemically reactive, pore structure, as occurs within an oxidizing body of graphite.

The conclusion is more-or-less forced: diffusion of oxidant (and products) in an oxidizing graphite body is best expressed in a Fickian format using an effective diffusivity, especially for low concentrations of diffusing gases where convective term is small. For example, impurity levels of oxidant, either O_2 or H_2O, may be as expected under normal operating conditions in a GCR, The next section shows that for such case, D_{eff} depends on the pore configuration and the diffusivities of the individual gases. Empirical D_{eff} values would therefore need to be evaluated for a range of burnoffs of interest and for each type of graphite.

There is an additional burden on proper evaluation of D_{eff} for high concentration of diffusing species, as expected for O_2 oxidation in an air ingress event. In such cases, the convective contribution to the transport is not negligible, and the Fickian format is technically inappropriate. Nevertheless, there appears to be no good alternative. In such case, estimation of the D_{eff} may require evaluation at various oxidation rates, as well as a range of burnoffs.

4.2 Physical Model for Effective Diffusivity

Consider the simple case of a slab of graphite of width, L, assumed to contain parallel pores extending from surface to surface. The pores, tubules actually, are assumed of uniform diameter and length ξL, where ξ, the tortuosity, is greater than unity. For this case, Hewitt and Morgan (1961) show for diffusion of a non-condensing gas in macropores,

$$D_{eff} = (\varepsilon/\xi^2)D_{gas},$$ (6)

where ε is the porosity. Equation (6) states that D_{eff} depends on the product of an internal structure parameter (the term in parentheses) and D_{gas}, the handbook value of the diffusing species in the gas mixture. Moreover, the structure parameter increases with burnoff (due to the ε in the numerator) from some low value at zero burnoff, approaching unity as the burnoff increases.

It should be recognized that ξ has no meaning for a porous body unless it is composed of continuous tubules. Therefore elaborate theories that add sophistication to this simple proposal are probably futile. In fact, most of the theoretical treatments of D_{eff} are elaborations of the simple tubule model.

8

The definition given by (6) results in odd units for D_{eff}, i.e., from (6) units are [(m³-void/m³-geom)/(m²-void/m²-geom)](m²-void/sec)], which simplifies to,

D_{eff} [units] = (m³-void)/(m-geom•sec).

This yields the correct units for diffusive flux,

J (mol O_2/m²-geom•sec) = D_{eff}(du/dx),

and the diffusive loss of oxidant from a volume element,

Diffusive loss (mol O_2/m³-geom•sec) = D_{eff} (du^2/d^2x,)

recalling that the units of u are mol O_2/m³-void.

Additional information presented by (6) is that D_{eff} should vary with temperature and pressure as does D_{gas}, the large volume value of the diffusing species in the gas mixture. For molecular diffusion, an ideal model predicts D_{gas} to be proportional to $T^{1.5}$ and diminishes with total pressure as P^{-1}. (As noted above, Knudsen diffusion and surface diffusion vary differently with temperature and pressure.) In this study, the $T^{1.5}$ temperature variation is assumed, and the pressure dependence is not activated.

4.3 Measured Values of Effective Diffusivity

The result of the uniform tubule model, limited to non-condensing macropores, is that D_{eff} may be expressed as

$D_{eff} = mD_{gas}$.   (7)

where m is a parameter that depends on the pore configuration, i.e., the burnoff, and D_{gas} is the handbook value for the diffusing species in the gas mixture. D_{gas} varies with absolute temperature approximately as $T^{1.5}$ according to a standard, basic correlation. In this formulation therefore, there is both burnoff and temperature dependence in $D_{eff.}$ (There is also a reciprocal variation with total pressure, which is not used in this study.)

Hewitt and Morgan (1961) measured the diffusivity of O_2, counter-diffusing with N_2 at room temperature. Specimens, 1-inch long by 0.5-inch diameter, were cut from a central region of a log of "Pile A" nuclear graphite. The diffusion direction of 1-inch was aligned in the direction of extrusion for nine specimens and transverse to the axis for 15 specimens, in some cases directly adjacent, for interesting comparisons.

Table 1 is a summary of their results. The numbers in parentheses are the number of data points for each case.

Table 1. D_{eff} Measurements for O_2 Counter-Diffusing with N_2,
Zero Burnoff at Room Temperature (Hewitt and Morgan, 1961)

Direction of	Value of m [Eq. (7)] x 100		
Diffusion	High	Low	Average

Parallel to axis of extrusion (9)	1.32	0.695	0.959
Perpendicular yo extrusion (15)	1.34	0.442	0.818

One measurement series was conducted at 400 °C to test the effect of a small degree of burnoff. No change in m was noted up to about 0.5% burnoff.

Hewitt and Sharratt (1964) reported values of m for five samples of British graphites, using the same technique and gases (O_2 counter-diffusing with N_2) as used by Hewitt and Morgan (1961). A summary isd shown in Table 2.

Table 2. D_{eff} Measurements for Four British Graphites; O_2 in N_2 at Room Temperature (Hewitt and Sharratt, 1964)

Graphite	m x 100
HX12	0.649
FPC	2.27
PGA	0.901
HX10	0.810

Hawtin et al. (1964), using a unique method, measured permeability and D_{eff} in an oxidizing graphite cylinder, 4.3-cm thick x 30-cm long. Air was the oxidizing gas at test temperatures of 435 – 485°C. The graphite was "British Pile A Graphite".

Their results showed an m value of 0.01 at zero burnoff, which remained virtually unchanged up to about 2% burnoff. Between 2% and 3% burnoff, there was gradual rise in m from 0.01 to about 0.013.

Hawtin and Gibson (1966) measured D_{eff} in oxidized "Pile A" British graphite in the temperature range 550 – 675°C. O_2 concentrations ranged from 2.5 – 20.8%. The graphite sample geometry and apparatus were the same as for Hawtin, et al (1964). m values were measured up to 20% burnoff.

They employed a complex analysis for determining m in the presence of a burnoff profile in a heavy-walled cylindrical tube. Results are presented as a calculated curve of $m\rho$ vs. %-burnoff. Table 3 shows the computed results, assuming the unoxidized density to be 1.8 g/cm^3.

Table 3. D_{eff} Estimates for a Thick-Walled Cylinder with a Pronounced Burnoff Profile (Hawtin and Gibson, 1966)

% Burnoff	m x 100
0	0.4
5	0.5
10	1

15	1.6
20	2.4

The cited burnoffs were estimated averages in the oxidized zone of the thick walled specimen. These D_{eff} results are lower than expected from previous measurements on Pile A Graphite. Because of the complexity of the analysis, it would be difficult to locate the cause of the difference.

Hawtin, Gibson, and Huber (1968) numerically estimated the average D_{eff} in a 14-foot long, 2-inch I.D., 8-inch O.D. annular test piece by fitting values in a differential equation to yield the observed overall oxidation rate. The oxidant was air. Temperatures ranged from 420 – 525°C. The graphite is described simply as "British Nuclear Grade". Table 4 is a tabular summary of their results, presented as a graph in their paper.

Table 4. D_{eff} Estimates of Hawtin, Gibson, and Huber (1968)

Overall Burnoff %	m x 100
0	0.9
1	1.1
2	1.4
3	1.9
4	2.5
5	3.2
6	4.0

4.4 Conclusions Regarding Use of Effective Diffusivity

• An effective diffusion coefficient in a Fickian format is a reasonable representation of multi-component diffusion in a porous body, especially for cases of low concentration of diffusing species.

• In such case, D_{eff} may be expressed as the product of a geometric term that varies with burnoff, idealized as ε/ξ^2 in the uniform tubule model, multiplied by, D_{gas}, the handbook value of the molecular diffusivity at the mixture composition.

• When transport occurs primarily in macropores,, defined as when Knudsen transport is negligible, D_{eff} should follow the temperature and pressure variation of the large volume diffusivity. That is, D_{eff} should vary as $T^{1.5}$ and as P^{-1}, as obtained from a standard idealized model. The $T^{1.5}$ variation is assumed for the illustrations below; the pressure effect is not used.

• Data for British nuclear graphites at low or zero burnoff and room temperature indicate that a D_{eff} of 1% of D_{gas} is a reasonable first estimate. This will be assumed as the nominal case for the illustrations below.

• The geometric factor, ε/ξ^2, as well as common sense, indicate that D_{eff} increases with burnoff, approaching the value of D_{gas} at some high value. Table 4 illustrates the rate of increase.

• Use of a Fickian effective diffusivity is a more difficult fit for higher concentrations of diffusing species (as for O_2 diffusion in an air ingress event), due to non-negligible diffusion-induced convection. However, there doesn't appear to be a reasonable alternative. In such cases, there is a greater burden on proper evaluation of D_{eff}, which may, in addition to internal structure, temperature and pressure, be a function of oxidation rate.

• The large literature on theoretical aspects of multicomponent diffusion in porous media is acknowledged. Many of the studies deal with conditions specific to catalyst pellets, i.e., prominent Knudsen diffusion in a non-reactive body; some involve condensing species. All seem to be elaborations of the parallel tubule concept, and introduce difficult-to-measure parameters. The results are invariably mathematically complex and seem inappropriate for general application to graphite oxidation.

5. SIMPLIFYING ASSUMPTIONS FOR OXIDANT TRANSPORT EQUATION

The following simplifications of the oxidant transport, equation (2), enable analytical solutions:

(1) <u>Quasi-steady State</u>. This assumption limits results to the fully developed profile. However, oxidation is never truly steady since material is being continuously removed. In effect we assume the fully developed profile moves inward slowly, without altering shape.

It can be shown that the quasi-steady profile is established rather rapidly at 800 K and above, for O_2 oxidation at least. This may be seen by assuming constant density in the oxidant transport equation (2) and recasting it as follows:

$$\partial u/\partial t = (D_{eff}/\varepsilon)\, u'' - (A/\varepsilon)\, u \qquad\qquad (8)$$

The prime denotes a derivative with respect to x. A is a material property proportional to the reactivity, but includes other parameters involved in determining the oxidant distribution, as defined below by (13a). Equation (8) is solved in Carslaw and Jaeger (1959) for the case of a semi-infinite slab with constant surface concentration and zero initial concentration. The solution is given in Appendix A, where it is used to derive the following relation between equilibration time and temperature,

$$T_{EQ,0.02} = 3.912\,(\varepsilon/2)\,A(T). \qquad\qquad (9)$$

$T_{EQ,02}$ is the time in seconds, required to achieve equilibration at the point where the equilibrium oxidant concentration is 2% of the surface value, i.e., at a location near the inner boundary of the active oxidation depth. Equation (9) is derived in Appendix A.[3] Equation (9) yields the following equilibration times, using preliminary kinetics constants for O_2 oxidation of a typical structural graphite for evaluation of $A(T)$:

Table 5. Equilibration Time (sec) vs. Temperature (K),
O_2 Oxidation of Typical Structural Graphite

Temperature	$T_{EQ,0.02}$
800	160
900	6
1000	0.5
1100-1400	< 1

---

[3] Equations given in Appendix A may be used to determine either (1) $u(x)$ profiles at selected times, or (2) time variation of $u(x)$ for a selected location, x, for the assumptions inherent in the treatment by Carslaw and Jaeger.

Equilibration times are predicted to be short for temperatures of 800 K and above, at least for O_2 oxidation. The trends however show that equilibration times increase rapidly at lower temperatures, and significantly longer times occur below 800 K. Also, equilibration times should be much longer for H_2O oxidation, due to lower reactivity.

An alternative method for estimating equilibration times involves comparing the mass of graphite removed within an active oxidation depth against the oxidation rate at the assumed temperature. This alternate method yields roughly comparable results.

Reasons for the short equilibration times for O_2 oxidation above 800 K are (1) the confinement of the active oxidation zone to a narrow width near the surface, and (2) the rapid increase in reaction rate with temperature.

(2) Constant D_{eff}

Since D_{eff} is a function of burnoff and hence of space, it must be placed within the divergence operator in (2). Although measurements reviewed above indicate only moderate variation with small degrees of burnoff, a fully developed oxidation profile encompasses a wide range of burnoffs, from perhaps 80% in a thin surface layer to 0% in the interior. Therefore, assumption of constant D_{eff} and a quasi-steady profile are in fact contradictory. Nevertheless, assuming constant D_{eff} for a semi-infinite slab leads to an exponential burnoff profile (see below) in qualitative accord with observed profiles (Katscher, 1988), albeit for unclear reasons.

In any case, the dependence of D_{eff} on burnoff is not known so there is no practical alternative at this time to assumption of constant D_{eff}.

(3) Linearized Oxidation Kinetics

The linearized form of (3) for O_2 oxidation takes the form,

$$R_1 = K_1 \exp(-H/RT) f(\alpha) P_{O2} \tag{10}$$

Simply setting the reaction order to unity while keeping the non-linear constants, leads to significant over-prediction of R_1 for O_2 pressures above about 50 Pa. Evaluating the constants K_1 and H for the linearized form minimizes the error, as was done in GDH (1988). Linearizing permits ready solution of oxidation rate and density profiles for simple geometries. It also permits easy coupling of the surface graphite oxidant concentration with the oxidant pressure in the free stream.

Using the ideal gas law for P_{O2} leads to

$$R_1(\underline{r},t) = K_1 \exp(-H/RT) f(\alpha) RT\, u(\underline{r},t) \tag{11}$$

For simplicity, u is used for the O_2 concentration in the voids, mol/m^3-void.

(4) Constant Graphite Density

The graphite density in the fully developed oxidation profile may vary from a remnant of about 10-20% of the unoxidized density at the exposed face, up the unoxidized density in the interior. The variation affects the value of the D_{eff}, $f(\alpha)$, and ε terms in several equations. We have already

14

assumed constant D_{eff} and quasi-steady state. Therefore an additional statement of constant graphite density applies only to the $f(\alpha)$ term in the kinetics equation.

Conclusion re simplifying assumptions: These assumptions permit easy survey of the effects of key parameters that affect the oxidation rate, e.g., (1) oxidant pressure in the free stream, (2) specimen size, (3) variation of D_{eff}, (4) effect of temperature, (5) buildup of H_2 in the interior for H_2O oxidation, and (6) comparison of structural vs. matrix type graphite. The results are, of course, approximate, but still deemed to be useful.

6. OXIDATION BY OXYGEN OF A SEMI-INFINITE SLAB

6.1 Oxidant Profile

Assume a semi-infinite slab with face $x = 0$ exposed to gas containing an oxidant of concentration U (mol/m^3), extending to infinity in the $+x$ direction. This geometry is more useful than seems at first since many oxidation depths above 800 K are on the order of millimeters, hence fairly small specimens can effectively be semi-infinite slabs.

The above assumptions permit writing the O$_2$ transport equation, (2), in x-geometry as,

$$0 = D_{eff}\, u'' - A\, u \tag{12a}$$

or more conveniently,

$$0 = u'' - B^2\, u \,. \tag{12b}$$

A is given by

$$A = K_1 \exp(-H/RT)\, f(\alpha)\, \rho N_{O2}\, RT \tag{13a}$$

and B^2 is defined as

$$B^2 = A/D_{eff} \tag{13b}$$

Equation (12) is a homogeneous, linear differential equation with constant coefficients, yielding solution by the characteristic equation method. Solution of the characteristic equation yields,

$$u(x) = C_1 \exp(-Bx) + C_2 \exp(Bx) \tag{14a}$$

C_2 is obviously zero since u must be finite at large x. C_1 may then be identified as the surface concentration, $u(0)$, resulting in,

$$u(x) = u(0) \exp(-Bx) \tag{14b}$$

In disguised form, the term $\exp(-Bx)$ is the well known Thiele equation and Bx the Thiele parameter. However, B includes contributory factors from its definition (13), not usually included in the Thiele parameter.

$u(0)$ is evaluated by equating the convection of oxidant to the surface to the diffusion of oxidant from the surface.

$$h_m(U - u_0) = -D_{eff}\, u'(\text{at } x = 0) \tag{15}$$

h_m is the mass transfer coefficient, U the free stream concentration of oxidant, u_0 the oxidant concentration in gas adjacent to the graphite surface. u_0 must be equal to $u(0)$, the oxidant concentration in the graphite at $x = 0$, because of the continuity of gas across the boundary into the graphite void space.

Evaluating the derivative at $x = 0$ and solving for $u(0)$, yields

$$u(0) = h_m U/(h_m + D_{eff} B) \tag{16}$$

Thus, the oxidant profile in a semi-infinite slab is given by (14) with $u(0)$ given by (16). The value of parameter B, containing $\exp(-H/RT)$, is low at low temperatures, in which case $h_m \gg D_{eff}B$, and (16) reduces as expected to

$$u(0) = U .$$

High temperatures, i.e. large B, place a large burden on O_2 transport to the surface. In such case $u(0)$ is reduced from the free stream value of U according to

$$u(0) = U (h_m/D_{eff} B).$$

The mass transfer coefficient, h_m, may be estimated by any appropriate correlation. The illustrations given in this memo assume low Reynolds number conditions typical of a small laboratory apparatus. Otherwise, there is no restriction of use of any other estimation of h_m for use in (16).

For the typical laboratory test, it is simplest to use the theoretical solution of a fully developed velocity and concentration profile for laminar flow in a tube (e.g., Hines and Maddux, 1985). Two limiting cases are (1) constant wall flux, in which the Sherwood number is evaluated as

$$Sh = 4.36,$$

and (2), constant wall concentration in which case,

$$Sh = 3.66.$$

Sh is defined as $h_m \cdot d_{hyd}/D_{gas}$, where d_{hyd} is the hydraulic diameter of the test section and D_{gas} is the diffusivity of the reactive gas in the free stream gas mixture. A rough average of $Sh = 4$ is taken between these two theoretical cases, which suffices for illustration purposes.

Therefore, mass transfer coefficients applied in the following illustrations are estimated from

$$h_m = 4D_{gas}/d_{hyd}. \tag{17}$$

Handbook values of D_{gas} for H_2O, H_2 and O_2 in helium are 2.74, 6.24 and 2.82 cm^2/sec at 400°C, respectively. In addition, simple kinetic theory of gases predicts a $T^{1.5}$ variation with temperature, which has also been included in these illustrations.

An implication of the temperature effect on D_{gas} is that the temperature variation will carry over to D_{eff}, i.e.,

$$D_{eff} = mD_{gas} \tag{7}$$

Thus D_{eff} in these illustrations is assumed to vary with temperature as $T^{1.5}$, an assumption that has not been shown to be the case.

Summary of the illustrative cases shown in this memo:

•All cases assume $m = 0.01$ for determination of D_{eff}, approximately as measured for zero or low burnoff for British nuclear graphite.

•For the O_2 oxidation cases, a free stream mixture of O_2/N_2 is assumed, with $D_{gas} = 0.849$ cm^2/sec at 673 K (HC&P, 2004) measured for an equi-molar mixture.

•For the H_2O oxidation cases, a free stream mixture of H_2O/He is assumed. D_{gas} is not conveniently listed in the HC&P for this composition. As an approximation, we will use the value for the equi-molar CH_4/He composition, which have approximately similar molecular weights. For this mixture $D_{gas} = 0.849$ cm^2/sec at 673 K (HC&P, 2004).

•D_{gas} will be assumed to vary with temperature as $T^{1.5}$, in correlations for both h_m and D_{eff}.

6.2 Surface Oxidation Rate of a Semi-Infinite Slab

The oxidation rate as observed at the $x = 0$ surface, R_3 in mol C oxidized/m^2.sec,[4] may be obtained by integrating the local rate given by (11), using the oxidant distribution given by (14), i.e.,

$$R_3 = \int_0^\infty R_1(x)\ \rho\ dx$$

Integrating from $x = 0$ to ∞ yields, after combining terms,

$$R_3 = Au(0)/(BN_{O2}) \tag{18}$$

Noting that $B^2 = A/D_{eff}$ leads to

$$R_3 = \sqrt{AD_{eff}}\ \frac{u(0)}{N_{O2}} \tag{19}$$

Since A contains the factor $\exp(-H/RT)$ and appears within the square root, the diffusion-limited surface oxidation rate, R_3, has an effective activation approximately equal to one-half the zone-1 rate. Equation (19) is the basis for this often-stated result.

However it is only approximately true because there are other temperature dependencies in (19). As seen from (13a), T also appears explicitly in A, and D_{eff} is expected to increase approximately as $T^{1.5}$. In addition, the surface concentration has a temperature dependence at high graphite reactivity i.e., high temperature. According to (16), at low reactivity, i.e., low B, h_m dominates the denominator and $u(0)$ is predicted to be equal to the free stream concentration, U. At higher reactivity (mainly higher T), the second term may dominate and $u(0)$ becomes dependent on the group $h_m/D_{eff}B$, which does depend on temperature.

Therefore, the generalization that the surface oxidation rate, R_3, has one-half the activation energy of the zone-1 rate is only approximately true.

---

[4] Nomenclature note: throughout, R_1 will signify oxidation rate per mole, e.g., mol C oxidized/mol C•sec, and R_3 the surface oxidation rate, mol C oxidized/m^2•sec.

Also (19) shows that increasing D_{eff} increases the surface oxidation rate, keeping all other parameters constant. The reason is that the depth of penetration of oxidant depends in part on D_{eff}. Increased penetration permits greater carbon exposure to oxidant, hence higher surface oxidation.

6.3 Graphite Density Profile

The quasi-steady state approximation assumes a nearly stable oxidant concentration profile, moving slowly inward while retaining its fully developed shape, ultimately leaving a remnant as the density wave moves inward. The graphite density profile in such case assumes the general character of the inverse of the oxidant profile.

The remnant density has been observed to be about 10-20% of the unoxidized density. The result of these considerations is the following relation between the graphite density and oxidant profile:

$$\rho(x) = \rho_{\infty} - (\rho_{\infty} - \rho_0)\,[u(x)/u(0)] \tag{20}$$

where ρ_0 is the density of "completely" oxidized remnant, and ρ_{∞} the unoxidized graphite. At large x in the interior of the slab, $u(x)$ approaches zero and $\rho(x)$ approaches the unoxidized value, $\rho\infty$. At the surface, $u(x) = u(0)$ and $\rho(x)$ assumes the value of the oxidized remnant, ρ_0. Thus, (20) predicts both limits properly.

Note that (14) predicts the $u(x)$ to be a diminishing exponential from the $x = 0$ surface. Consequently, the graphite density profile (20) takes an inverse form, predicting $\rho(x)$ to be a minimum of ρ_0 at the surface, increasing as $(1 - \exp(-Bx))$, asymptotically approaching ρ_{∞} at some point in the interior.

Equation (20) may be readily recast into burnoff profile terminology by noting,

$$BO = 1 - \rho/\rho_{\infty},$$

where BO is the fractional burnoff.

6.4 Effect of D_{eff} on Semi-Infinite Slab Profiles

The simple semi-infinite slab geometry is convenient for illustrating effect of D_{eff} on density and oxidant profiles. The following oxidation constants for a typical structural graphite and fuel matrix will be assumed, obtained in preliminary tests.

Structural Graphite
$K_1 = 3.89$ 1/sec.Pa
$H = 186,960$ J/mol

Fuel Matrix Graphite
$K_1 = 3.73$ 1/sec.Pa
$H = 160,420$ J/mol

These constants are used to calculate A and B in (13a) and (13b). As above, D_{eff} is assumed in the form

$$D_{eff} = m \, D_{gas}$$

where m is an empirical constant, which may range from 0.1% to 5%, and D_{gas} is an estimate of the handbook value for the gas oxidant composition. A temperature variation of D_{gas} as $T^{1.5}$ is predicted in correlations.

Assuming a specimen temperature of 1000 K, a free stream partial pressure of 3000 Pa O_2, and a laminar flow mass transfer coefficient from (17), yields the O_2 profiles for a range of assumed D_{eff}'s shown in Fig. 1. As seen, a D_{eff} of 1% of D_{gas}, roughly as measured by Hewitt and Hawtin, yields a profile extending to a depth of about 5 mm.

This agrees fairly well with the burnoff profiles measured by Katscher (1988) for German structural graphites A3-3 and A3-27, taking the measurements closest to 1000 K. These generally show oxidation depth of from 4 to 5 mm in good agreement with Fig. 1. However, this is a bit misleading as Katscher's tests used O_2/He, compared with O_2/N_2 assumed for Fig. 1. The lower D_{gas} of O_2/N_2 should have calculated a narrower depth than the 4-5 mm shown in the figure.

Fig. 1 O2 Concentration vs. Depth
Semi-Infinite Slab, Structural Graphite, PO2=3000 Pa, 1000K
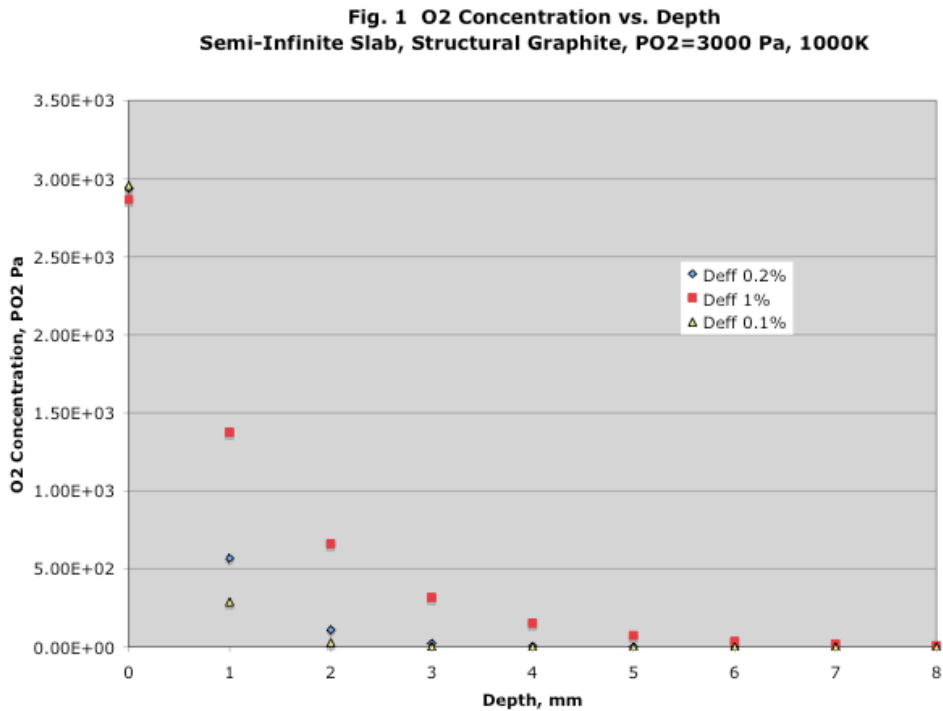
In contrast, Contescu (2008) reports much shallower oxidation depths, approximately 1 mm at 1000K for a typical structural graphite oxidized in air. Such a shallow depth is representative of a much lower D_{eff} value than expected, approximately m = 0.1%. The cause of the difference is not clear.

However, at this stage we are merely reviewing older concepts by presenting some examples. Resolution of differences between calculation and various observations resulting from uncertainties in D_{eff} or approximations of the calculations are not the main objective at this time.

However it seems, at least from the profiles of Katscher, that profiles based on the linearized transport equation and the D_{eff} measurements reported in the AERE reports are generally in accord.

Fig. 2 Density Profiles, Range of Deff Values
3000 Pa O2, Structural Graphite, Semi-Infinite Slab, 1000 K
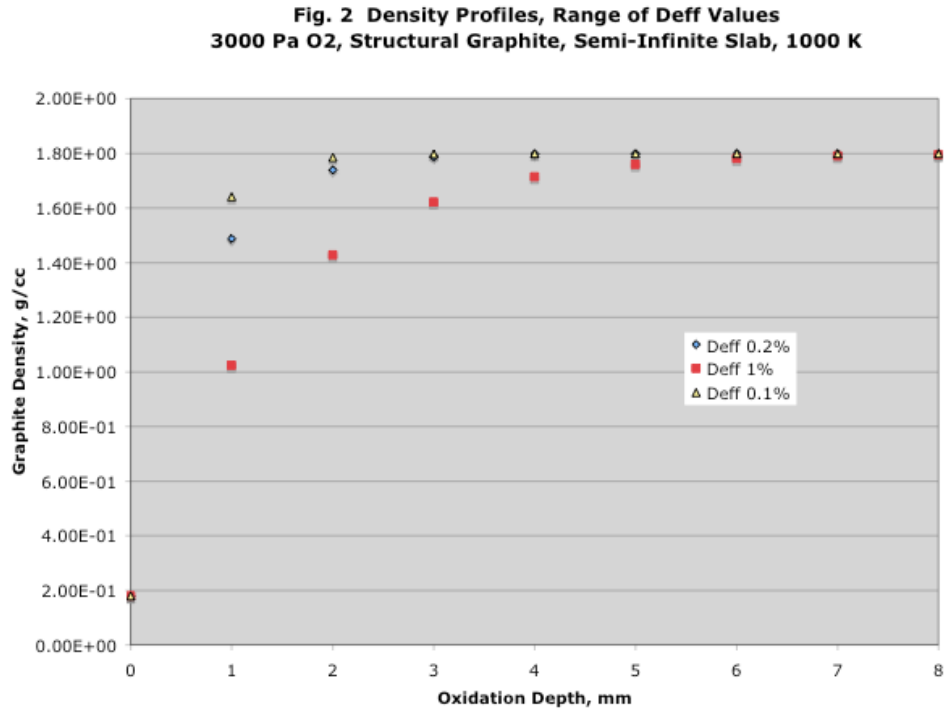

Figure 2 shows the transposition of the O_2 concentration profile of Fig. 1 into the graphite density profile, based on equation (20). As seen in the figure, a density of 0.2 g/cm^3 is assumed for the surface remnant, compared with the unoxidized density of 1.8 g/cm^3 in the interior.

7. OXIDATION BY OXYGEN OF A FINITE SLAB

7.1 Oxygen Concentration Profiles in a Finite Slab

The general solution, (14a), applies also to the finite slab, but is more conveniently written,

$$u(x) = C_1 \sinh(Bx) + C_2 \cosh(Bx) \tag{21}$$

The boundary conditions are:

BC 1: $u'(L) = 0$ (symmetry)
BC 2: $h(U - u_0) = -D_{eff} u'$ at $(x=0)$

where L is the half-width of the slab. Application of BC 1 leads to

$$C_1 = -C_2 \tanh(BL)$$

Substitution into (21) leads to the oxidant concentration profile for the finite slab,

$$u(x) = u(0)[\cosh(Bx) - \tanh(BL)\sinh(Bx)]. \tag{22}$$

C1 has been recognized to be $u(0)$, which is evaluated from the surface boundary condition. Application of BC 2 to (22) leads to,

$$u(0) = h_m U/[h_m + D_{eff} B \tanh(BL)] \tag{23}$$

Hence, the O_2 profile in a finite slab of half-width L is given by (22), with the surface concentration given by (23).

The surface oxidation rate, R_3, for a finite slab is obtained by integrating the diffusion-unaffected oxidation rate, (11), from $x = 0$ to L, using the finite slab O_2 profile, (22). Carrying out the integration and simplifying leads to

$$R_3 = Au(0)\tanh(BL)/(N_{O2}B), \tag{24}$$

where $u(0)$ is given by (23). The units of R_3 are mol C oxidized/m^2 surface per second.

We note again that (24) predicts an activation energy approximately equal to one-half the diffusion-unaffected activation energy, since the ratio A/B contains the term $\sqrt{(\exp{-H/RT})}$. It is again only approximate because there are other temperature variations: in u(0) depending on the value of h$_m$, and also in the term tanh(BL).

7.2 Oxidation Efficiency and a Zone-1 Criterion

The oxidation efficiency defines how closely a supposed zone-1 sample (i.e., one designed for uniform oxidation) actually approaches zone-1 conditions. The term is analogous to "catalyst efficiency" or "catalyst effectiveness factor" which is an estimate of how fully a catalyst is utilized. Equation (24) may be adapted for this purpose as follows:

The oxidation rate per unit mass of sample of half-thickness, L, is equal to the surface rate divided by $\rho \cdot L$,

$$R_1(\eta) = R_3/(\rho L) \tag{25}$$

In (25) $R_1(\eta)$ is the oxidation rate per unit mass in the sample accounting for the actual oxidant profile, not the ideal flat profile. Therefore, dividing (24) by ρL yields after some re-arranging,

$$R_1(\eta) = [Au(0)/(\rho N_{O2})]\,[\tanh(BL)/BL]. \tag{26a}$$

Note that if the value of the term in brackets were unity, then $R_1(\eta)$ would be equal the uniform oxidation rate at the uniform concentration of $u(0)$. The term in brackets may be called the oxidation effectiveness factor, i.e.,

$$\eta = \tanh(BL)/BL \tag{27}$$

Alternatively, the oxidation rate per unit mass of specimen, may be rewritten as,

$$R_1(\eta) = \eta\, Au(0)(\rho N_{O2}). \tag{26b}$$

L'Hopitals's Rule may be used to show that

Limit [tanh x/x] as x$\rightarrow$ 0 equals 1,

which defines the theoretically unobtainable perfect zone-1 condition. When $\eta < 1$, diffusion limits the oxidation to less than uniform utilization of the entire sample. Zone-1 conditions are approached when either L approaches zero, and/or B, representing the oxidation rate divided by the effective diffusivity, approaches zero. Thus, $BL \rightarrow 0$ defines the perfect zone-1 condition. The value of η vs. BL is illustrated in Fig. 3.

Fig. 3 Oxidation Effectiveness Factor vs. BL
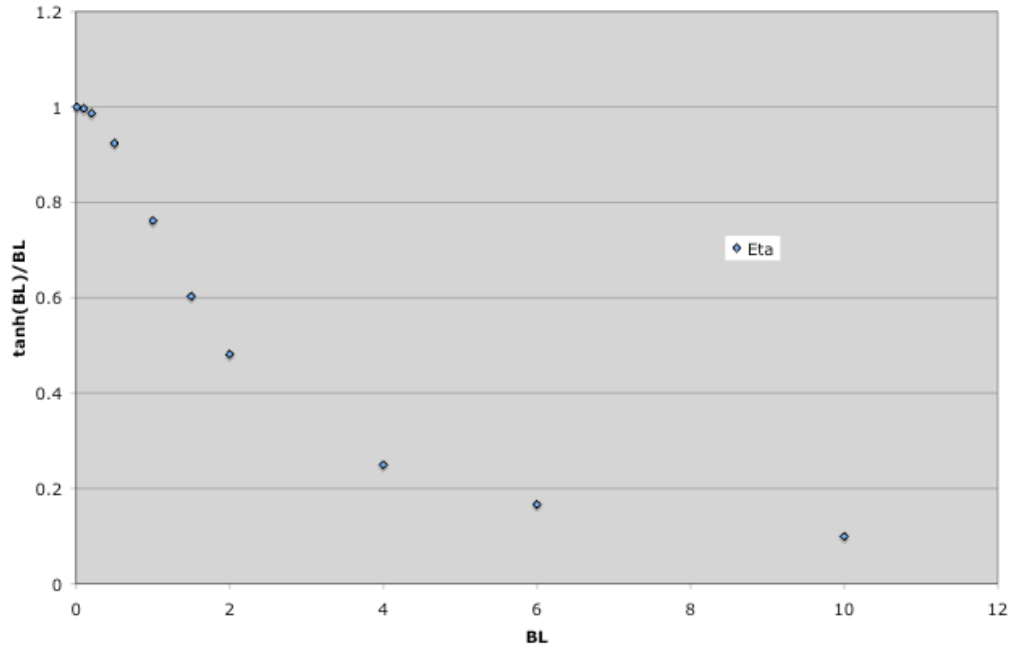
Note that values of *BL* less than about unity yield oxidation effectiveness factors of 80% and above. Therefore we may write a zone-1 criterion,

$$\text{Zone-1 Criterion for a Slab:} \quad BL < 1 \ . \tag{28}$$

Using an early estimate of kinetics parameters to evaluate *B*, (28) may be used to bracket in a reasonable range of zone-1 experimental conditions. If a particular test proves to be less than ideal, i.e., $\eta < 1$, as will usually be the case, (26) may be used to provide a correction to the data, accounting for the non-ideal oxidant profile.

Figure 4 shows the variation of *h* with temperature for a 0.5-cm thick sample of typical structural graphite, using preliminary estimates of kinetic parameters. As seen, zone-1 conditions are approximately met for this width for temperatures up to about 950 K, at which point the oxidation effectiveness dips below 80%.

Fig. 4 tanh(BL)/BL for 0.5cm Width Slab
Structural Graphite
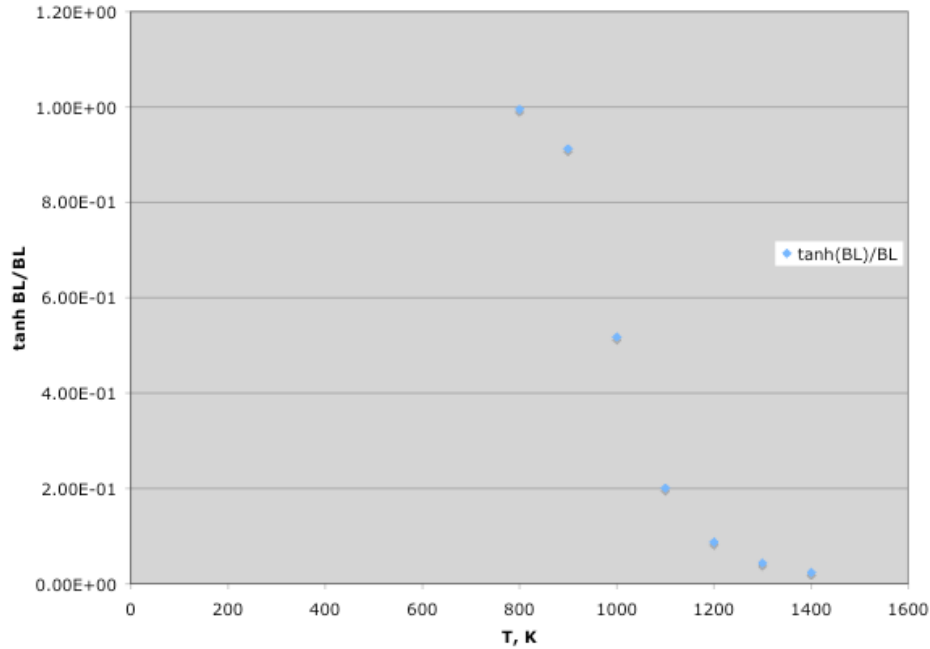
In section 9 the oxidation efficiency is developed for the long cylinder and values compared for O_2 and H_2O oxidation. It is shown that in general oxidation efficiencies are lower for O_2 oxidation, other parameters kept equal, due to the higher reactivity of O_2 vs. H_2O.

Analyses of oxidation efficiency are based on earlier studies of the equivalent concept, the catalyst effectiveness factor. For example, Weisz and Prater (1954) derive a factor equivalent to (27) and a zone-1 condition equivalent to (28). Petersen (1965) is one of several who extend the analysis to more complex situations. Petersen includes a nonlinear oxidation model. The reader is welcome to try a hand at deciphering the complex development that ensues. In the modern context, such mathematical gyrations are best replaced by complete and uncompromised computer solutions based on the general oxidation equation (1). Meanwhile simple criteria such as (27) and (28) provide ready approximation of the degree of approach to uniform oxidation for simple geometry.

7.3 Illustrated Cases for Oxidation by Oxygen of Finite Slab

Some applications of the finite slab equations are shown in the following figures. Preliminary kinetics constants for a typical structural graphite and fuel matrix graphite listed in section 5.4 are assumed. Also assumed are a free stream O_2 partial pressure of 3,000 Pa and a total sample width of 0.5 cm.

Equation (23) may be used to determine the onset of surface O_2 depletion, when the total oxidation rate in the sample taxes the convection capability of O_2 to the surface. As seen in (23), the ratio $u(0)/U$ depends on the mass transfer coefficient, h_m, and on all factors affecting the total oxidation rate, i.e., D_{eff}, which affects the depth of oxidation, the kinetics constants embedded in B, and the specimen half-width, L.

25

The value of h_m is determined, for illustrative cases in this memo from (17), appropriate for a laboratory apparatus. D_{gas} for O_2 in He is 2.82 cm²/sec at 400°C for a 50/50 mixture of O_2/He, and a $T^{1.5}$ dependence on temperature is assumed.

Assumption of $D_{eff} = m \cdot D_{gas}$ places both a burnoff-dependence (in m) and a temperature-dependence (in D_{gas}) for D_{eff}. In all cases in this section, a value of $m = 0.01$ is assumed, approximately the value reported for zero burnoff in British nuclear graphite (see section 3).

Figure 5 shows the ratio of the surface oxygen to free stream concentration vs. temperature for a typical structural graphite and fuel matrix graphite. For this case, $u(0)$ is seen to be equal the free stream concentration for temperatures up to about 1000 K. But for matrix material, $u(0)$ would require a correction from the free stream value for temperatures above about 800 K. The basis for correction would be Eq. (23) with the proper estimated h_m.

If the constant m were less than 0.01, which may well be the case, surface O_2 depletion would occur at a higher temperature due to a shallower oxidation profile, and consequently a lower surface oxidation rate.

Figure 6 illustrates another type of zone-1 test, (besides the oxidation efficiency method) comparing the surface oxygen concentration to the value at the mid-plane. The figure plots the ratio $u(0)/u(L)$ vs. temperature. The result is consistent with the oxidation efficiency method shown in Fig. 4, showing strong departure from the ideal zone-1 condition at temperatures above 900 K for a typical structural graphite and 800 K for a fuel matrix graphite.

Fig. 5 Oxygen Starvation Test
0.5 cm Specimen, Deff = 1%
Free Stream O2 = 3000 Pa in He
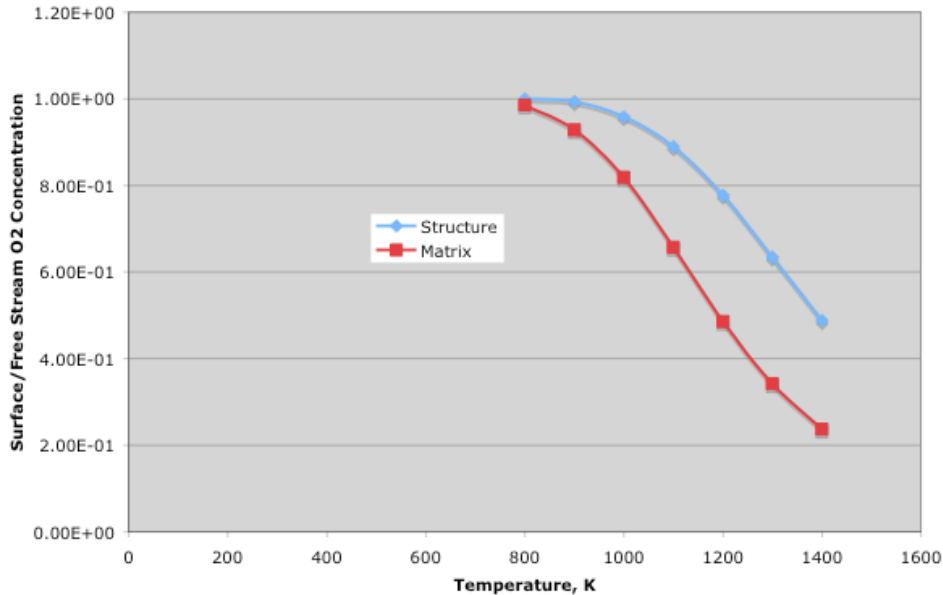
Fig. 6 Zone-1 Test, Center/Surface O2 Concentration
0.5 cm Width, Deff = 1% D Hndbk
PO2 = 3000 Pa in He
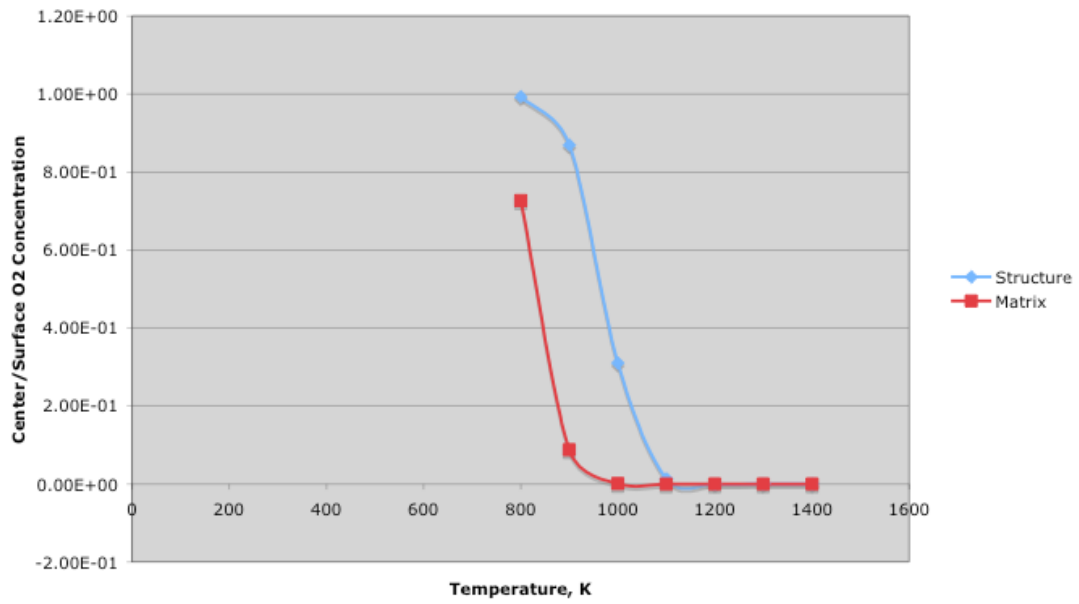
Figure 7 shows the variation of the surface oxidation rate vs. temperature, using (24). As shown below, when plotted in the conventional Arrhenius manner, an effective activation energy of approximately *H*/2 is approached at high temperature. However, this idealization is only approximately true due to other temperature influences in (24).

Fig. 7 Surface Oxidation Rate, Stuctural and Matrix Graphite
Deff = 1%, PO2 = 3000 Pa in He
Specimen width = 0.5 cm
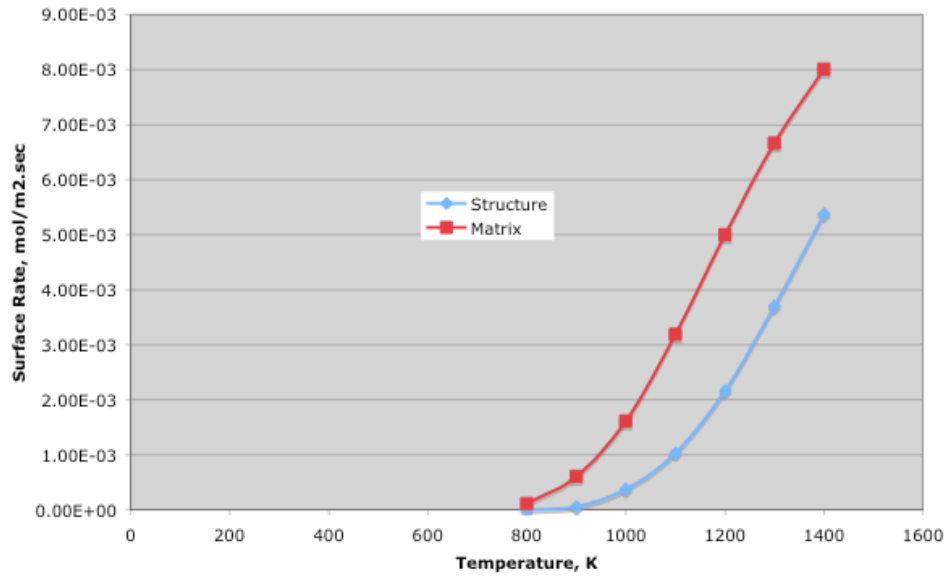
8. OXIDATION BY OXYGEN OF AN INFINITE CYLINDER

8.1 Oxygen Concentration Profile in an Infinite Cylinder

The equivalent of (12a) written for cylindrical coordinates is,

$$0 = D_{eff} (1/r)\, d/dr(r\, du/dr) - Au \tag{29a}$$

where u again is the O_2 concentration in the graphite pores at location r, and A has the same definition as in (13a). Dividing by D_{eff} and defining B as in (13b) yields the more convenient form,

$$0 = (1/r)d/dr(r\, du/dr) - B^2\, u \tag{29b}$$

Equation (29b) is a Bessel equation with solution

$$u(r) = C_1\, I_0(Br) + C_2\, K_0(Br)$$

I_0 and K_0 are the zero order modified Bessel functions of the first and second kind, respectively. Since $K_0(Br)$ goes to infinity as Br approaches zero, C_2 must be zero. And since $I_0(Br)$ equals unity at $Br = 0$, C_1 may be identified as $u(0)$, the O_2 concentration at the centerline of the cylinder. Therefore,

$$u(r) = u(0)\, I_0(Br). \tag{30a}$$

Setting $r = a$ yields the surface concentration, $u(a)$,

$$u(a) = u(0)\, I_0(Ba)$$

which when substituted into (30a) yields,

$$u(r) = u(a)\, I_0(Br)/I_0(Ba) . \tag{30b}$$

Evaluation of $u(a)$ requires application of the surface boundary condition. Equating the convection rate of O_2 to the surface with the diffusion of O_2 from the surface,

$$h_m (U - u(a)) = -D_{eff} (du/dr),\ \text{at } r = a \tag{31}$$

where a is the radius of the cylinder. As for the slab, the O_2 concentration in the gas at the surface must equal $u(a)$, the concentration in the graphite at the surface, because of the continuity of gas space across the boundary.

Taking the derivative using (30b), evaluating it at $r = a$, and substituting into (31) leads to the expression for the surface concentration of O_2.

$$u(a) = h_m\, U/[h_m + D_{eff}\, B\, (I_1(Ba)/I_0(Ba))] \tag{32}$$

The function I_1 is the first order Bessel function of the second kind. Equation (30b), using $u(a)$ from (32), defines the O_2 concentration profile in the cylinder.

8.2 Surface Oxidation Rate for a Cylinder

The surface oxidation rate, R_3 mol C oxidized per meter length of rod per second, is evaluated from,

$$R_3 = \int_o^a R_1(r) \ r \ 2\pi r \ dr \qquad (33)$$

integrating from $r = 0$ to a. R_1 is the diffusion-unaffected oxidation rate per (11). Substituting for R_1 and using the oxidant profile from (30) yields on integrating,

$$R_3 = (2\pi a/N_{O2}) \ u(a)(A/B) \ I_1(Ba)/I_0(Ba) \qquad (34)$$

Note that the temperature dependence of R_3 for the cylinder is approximately as given for the slab, $\exp(-H/2RT)$, i.e., an Arrhenius dependence with one half the activation energy of the diffusion-unaffected value. This is due to the ratio (A/B) and definitions of A and B. However, again, this is only approximately true because of the several other temperature dependencies in (34), i.e., in B and possibly in surface concentration, $u(a)$, depending on the reactivity and specimen size.

8.3 Oxidation Efficiency for a Cylinder

The oxidation efficiency for a cylinder is determined by dividing the diffusion-limited R_3 of (34) by an assumed uniform oxidation rate,

$$R_3 \ (\text{uniform}) = R_1(a) \ \rho \ \pi a^2, \qquad (35)$$

evaluated using the O_2 concentration in the graphite as constant at the surface value, $u(a)$.

Dividing (34) by (35) and simplifying using the definitions of A and B yields the oxidation efficiency for a cylinder:

$$\eta = (2/Ba) \ I_1(Ba)/I_0(Ba). \qquad (36)$$

Equation (36) is derived in standard texts, e.g., Coulson and Richardson Vol. III (1991).

The variation of η with specimen size and the parameter, B, which contains the kinetic constants and D_{eff}, is much the same as for the finite slab (Eq. (27) and Fig. 3), as seen in Fig. 8 for the cylinder.

Fig. 8 Oxidation Efficiency vs Ba, Cylinder

Fig. 8 Oxidation Efficiency vs Ba, Cylinder
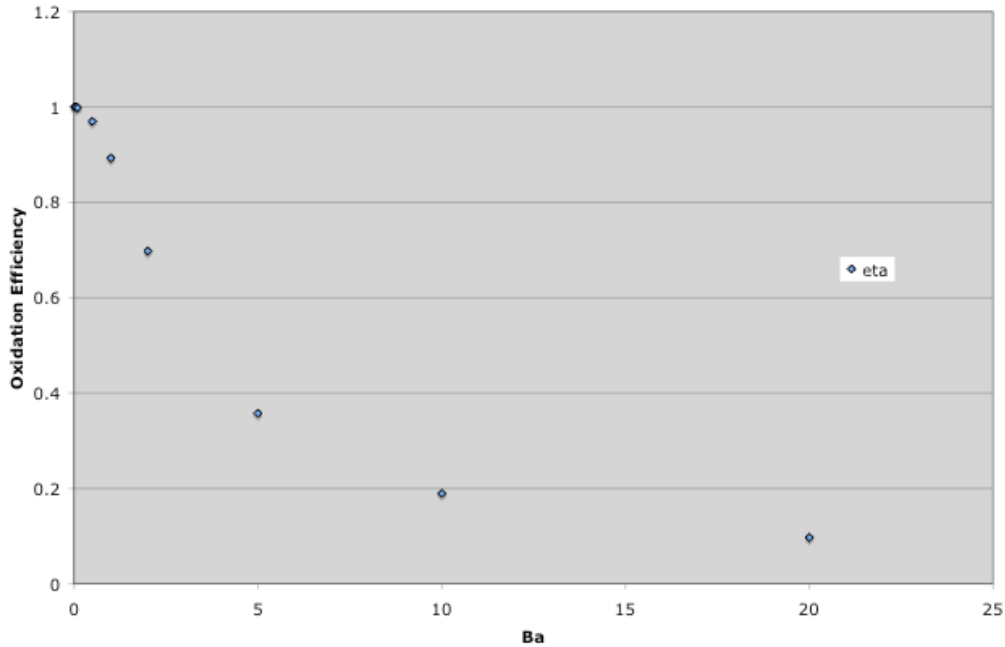
Small B signifies low reaction rate and/or high D_{eff}, both leading to uniform oxidation, i.e., $\eta = 1$. Also, diminishing specimen radius, a, tends toward uniform oxidation. Clearly then, as $Ba \rightarrow$ zero, $\eta \rightarrow 1$, as confirmed in the figure. If we define zone-1 for a cylinder when $h > 0.9$, then Ba < 1 is an approximate zone-1 criterion for cylindrical specimens.

8.4 Temperature Dependence of Surface Oxidation Rate

The temperature dependence of the surface oxidation rate, R_3, has been shown for the slab in Fig. 7. The variation for the cylinder plotted on Cartesian coordinates appears much the same.

R_3 in the diffusion-affected zone has an approximate Arrhenius dependence with temperature with an activation energy one-half of the uniform oxidation value. Looking at the temperature dependent terms in (34) a bit more closely shows some additional detail:

•The principal temperature dependency comes from the ratio A/B, which has the term exp(-H/2RT), where H is the zone-1 activation energy. Figure 9, shows the predicted variation of log(R_3) with $1/T$ using Eq. (34) for a typical structural graphite and fuel matrix. Other temperature effects alter the effective activation energy over the temperature range. The dark line with triangle points is the theoretical line with effective activation energy of $H/2$. The other two lines are calculated using (34) for a typical structural graphite and a carbonaceous matrix.

•The ratio A/B also contains the factor $\sqrt{D_{eff}}$. D_{eff} has been assumed to be given by $m \cdot D_{gas}$, where D_{gas} varies with temperature as $T^{1.5}$. Therefore this term places a $T^{0.75}$ variation in R_3. (However, the $T^{1.5}$ temperature variation of D_{eff} has not been demonstrated).

•A/B also contains the factor $\sqrt{T}$, arising from the conversion of P_{O2}, the approximate oxygen activity, to concentration units using the ideal gas law.

•The factor $\sqrt{N_{O2}}$ also occurs in A/B, which may vary from unity at low temperature and excess O_2 to 0.71 at high T or in a low O_2 concentration. This feature was not activated in the approximations for Fig. 9.

•The term $u(a)$, the surface concentration of O_2, also occurs in R_3. As seen from (32), there are several possible temperature influences in $u(a)$. At low temperature, $u(a)$ varies approximately as h_m, which in laminar flow is proportional to D_{gas}, and therefore as $T^{1.5}$. At high temperature, $u(a)$ varies as $h_m/(D_{eff} \cdot B)$. Therefore, at high temperature the temperature variation in $u(a)$ approximately cancels out, leaving the principal temperature effect of A/B. Hence we see in Fig. 9 that R_3 approaches the theoretical variation of $\exp(-H/2RT)$ at high temperature, at least for a typical structural graphite beginning at about 1400 K.

Fig. 9 Log Surface Rate vs. 1/T
0.5 cm Cylinder, 3000 vpm O2
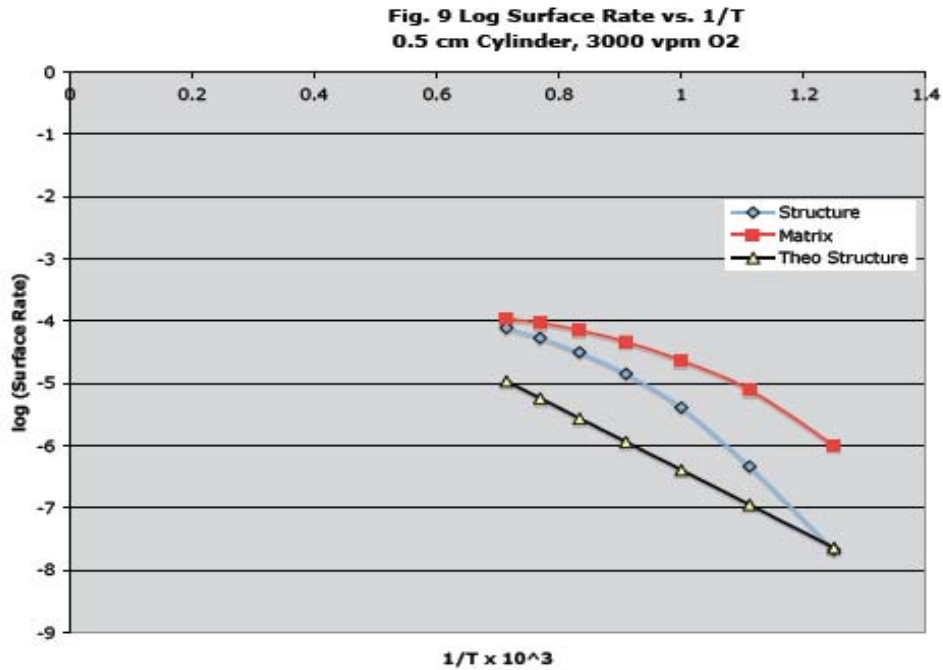
8.5 Oxidant and Density Profiles in a Cylinder

O_2 concentration profiles for the cylinder may be portrayed using (30) and (32), which can be converted to graphite density profiles using (20). In addition, surface to center concentration ratios, zone-1 criterion parameters, and surface concentration depletion effect vs. temperature may be plotted using the equation developed in section 7. In general, the variations for the cylinder are quite similar to that already shown for the finite slab. Calculation of these curves is equally convenient since numerical values for the required Bessel functions are given in the popular spreadsheet programs, e.g., Excel.

9. OXIDATION BY MOISTURE AND HYDROGEN BUILDUP IN A FINITE SLAB

9.1 Coupled Transport Equations for Water and Hydrogen

The kinetics equation for H_2O oxidation of graphite is often given in the Langmuir-Hinshelwood form,

$$R_1 = K_1 P_{H2O}/[1 + K_2 P_{H2}^n + K_3 P_{H2O}] \tag{37}$$

Units of R_1 are mass C oxidized/mass sample sec. The K's are the temperature-dependant pre-multipliers,

$$K_1 = K_{W1} \exp(-H_{W1}/RT)$$
$$K_2 = K_{W2} \exp(-H_{W2}/RT)$$
$$K_3 = K_{W3} \exp(-H_{W3}/RT).$$

The order, n, on P_{H2} is sometimes used, estimated to be 0.75, with large experimental uncertainty. Since n would be the 7th empirical parameter in the rate equation, its practical utility may be questioned. Values for the seven parameters in (37) are reported by Burnette (1978) for H451 graphite. Two sets of quite different parameters are given in this reference for P_{H2O} ranges above and below 300 Pa.

The oxidation inhibition by H_2 shown in (37) is a small nuisance for the experimentalist, but a more formidable problem for the analyst dealing with large graphite members where the H_2 concentration may build with depth. A sufficiently small specimen for a zone-1 experiment is one where the H_2O concentration is assured constant and equal to the free stream value. In such case, the H_2 concentration would also be expected to be constant at the experimentally fixed free stream value since H_2 has a significantly higher diffusivity than H_2O.

For large members typical of structure, moderator or matrix graphite, assumption of uniform internal H_2 concentration equal to the free stream value may not be valid. In such case, ideally, the H_2O and H_2 transport equations should be solved simultaneously. Using the simplifying assumptions stated in section 4, except linearization of the kinetics equation, the coupled H_2O, H_2 transport equations may be written,

$$0 = D_u \nabla^2 u - R_1 \rho N_{H2O} \tag{38}$$

$$0 = D_v \nabla^2 v + R_1 \rho N_{H2}. \tag{39}$$

Definitions for (38) and (39) are as follows:

D_u, D_v	effective diffusivities for H_2O and H_2
u	moles H_2O/m^3-void
v	moles H_2/m^3-void
N_{H2O}	moles H_2O consumed per mole C oxidized
N_{H2}	moles H_2 produced per mole C oxidized

Equations (38) and (39) are coupled because u and v are both contained in R_I, the diffusion-unaffected oxidation rate; R_I is the source for H_2, which in turn has an inhibiting effect on the oxidation rate. Linearizing R_I, as assumed in section 8.4, permits only sequential solution for u and v, but does not portray the true inhibiting effect of H_2.

9.2 Effect of Hydrogen Inhibition and Linearization

The linearized version of the H_2O oxidation equation is written,

$$R_I = K_I \, P_{H2O} \tag{40}$$

and $RT \cdot u$ may be substituted for P_{H2O} in the oxidant transport equation. Linearizing uncouples (38) and (39) and permits sequential estimation of the H_2O and H_2 concentration profiles in graphite.

The error due to linearization may be estimated by taking the ratio of (40) relative to (37), i.e.,

$$R_I(\text{linear})/R_I(\text{nonlinear}) = 1 + K_2 \, P_{H2}^{0.75} + K_3 P_{H2O}.$$

Table 6 shows the fractional error to R_I(nonlinear) due to linearization using the low H_2O pressure ($P_{H2O} < 300$ Pa) kinetics constants of Burnette (1978) for H451.

Table 6. Ratio, Linear/non-Linear H_2O Oxidation Rate
(with no modification of K_I)
(H451, Low P_{H2O} Range, $P_{H2O} < 300$ Pa)

Temp, K	P_{H2O}	P_{H2}	Rate Ratio
1000	300	0	1.6
1000	300	150	2.2
1200	80	0	2.1
1200	60	10	2.1
1200	40	30	2.2

Burnette's constants for the high P_{H2O} range ($P_{H2O} > 300$ Pa) are such that the ratio R_I(linear)/ R_I (non-linear) is virtually unity for all reasonable temperatures and P_{H2}, P_{H2O} partial pressures.

In sum, in the low partial pressure regime, linearized rates are about a factor two higher than the non-linear rates up to 1000 K. At 1200K, H_2O partial pressures must be held to about 50 Pa so as not to exceed a factor of two error. However, the accuracy of the linearized estimated rates may be improved by revision of K1 to a lower value.

At high H_2O pressures ($P_{H2O} > 300$ Pa), according to the rate constants of Burnette, there is virtually no linearization error for all reasonable temperatures and pressures.

9.3 Comparison of Oxidation Rates by Oxygen and by Water

The zone-1 oxidation rates for O_2 and H_2O are compared in Fig. 10. Rate constants for O_2 oxidation of H327 graphite were taken from GDH (1988); rate constants for the Langmuir-Hinshelwood equation for moisture oxidation were taken from Burnette et al (1978)[5].

Two curves are shown for oxidant pressures of 200 and 2000 Pa, and zero H_2 partial pressure for H_2O. As seen, O_2 oxidation rates generally far exceed H_2O rates for equal oxidant pressures, especially at low temperatures. At 900 K, O_2 rates are predicted to be 500 times the H_2O rate for oxidant pressures of 200 Pa. At higher oxidant pressure of 2,000 Pa, the ratio is 500 at 900 K.

Since O_2 and H_2O effective diffusivities are not expected to be vastly different, the higher oxidation rates for O_2 signify much shallower oxidation penetration relative to H_2O.

Fig. 10 Oxidation Rate Ratios, O2 vs. H2O Rate
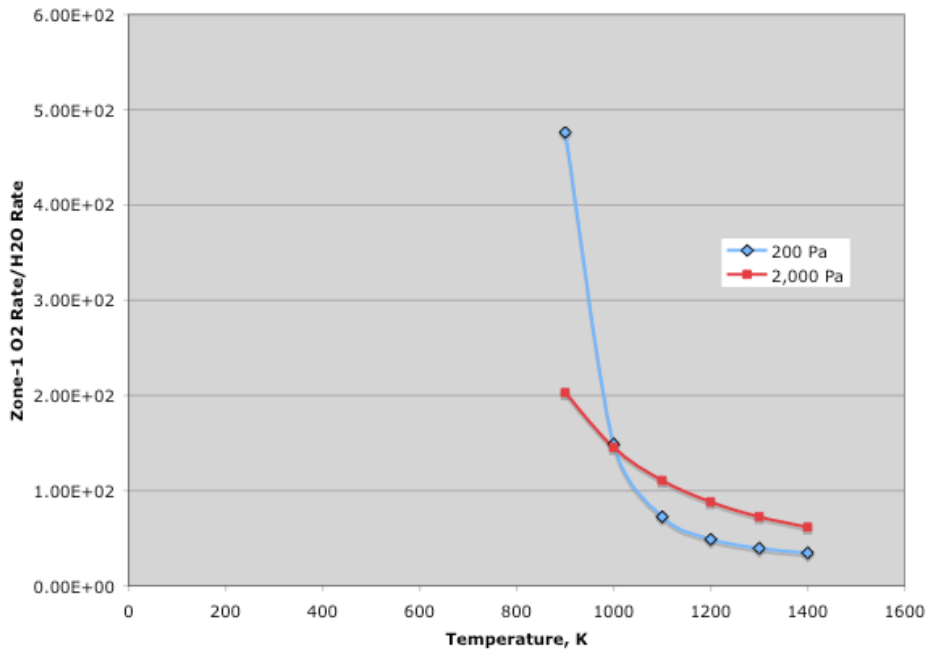
9.4 Estimation of Water and Hydrogen Concentration Profiles in a Finite Slab

Linearizing the kinetics term in the quasi-steady state H_2O and H_2 transport equations decouples them. For the slab, the H_2O and H_2 balances, Eqs. (38) and (39), become,

$$0 = D_u u'' - A_u u \tag{41}$$

$$0 = D_v v'' + A_v u. \tag{42}$$

---

[5] First author of the report is actually C. Velasquez. However R.D. Burnette was the well-known group leader of graphite oxidation work at GA. The report is better known listing his name first.

The terms, A_u and A_v, are similar to that defined for O_2 oxidation except here with stoichiometric parameters N_{H2O} and N_{H2} in A_u and A_v, respectively, instead of N_{O2}, i.e.,

$$A_u = K_1 \exp(-H/RT) \; r \; N_{H2O} \; RT \qquad (43a)$$

$$A_v = K_1 \exp(-H/RT) \; r \; N_{H2} \; RT \qquad (43b)$$

Or in the more convenient form,

$$0 = u'' - B_u^2 \, u \qquad (44)$$

$$0 = v'' + B_v^2 \, u, \qquad (45)$$

where $B_u^2 = A_u/D_u$ and $B_v^2 = A_v/D_v$. The H_2O profile, $u(x)$, is the same as for the slab (22), however with the different definition of B,

$$u(x) = u(0)[\cosh(B_u x) - \tanh(B_u L) \sinh(B_u x)] \qquad (46)$$

The H_2 profile is obtained by substituting (46) into (45) and integrating twice.

$$v(x) = v(0) + u(0)(B_v^2/B_u^2) \, [1 - \cosh(B_u x) + \tanh(B_u L) \sinh(B_u L)] \; . \qquad (47)$$

$u(0)$ and $v(0)$ are the concentrations of H_2O and H_2 in the graphite at the $x = 0$ surface exposed to the free stream. As for O_2, the surface concentrations are obtained by equating the convective delivery rate of H_2O to the surface, and the convective removal rate of H_2 from the surface to the diffusion rates in the graphite at the surface; i.e.,

$$h_u(U - u(0)) = D_u \, u' \text{ (at } x = 0), \qquad (48)$$

and for H_2,

$$h_v(v(0) - V) = D_v \, v' \text{ (at } x = 0). \qquad (49)$$

U and V are the free stream concentrations of H_2O and H_2, respectively. As before, $u(0)$ and $v(0)$, the H_2O and H_2 concentrations in the graphite at the surface, are equal to the H_2O and H_2 concentrations in the gas at the surface because of the continuity of gas space across the boundary into the graphite voids.

Since convection rates are usually in the laminar regime, at least in laboratory equipment, and hence depend on diffusivity, we must distinguish between the H_2O mass transfer coefficient, h_u, and that for H_2, h_v.

Evaluating $u'(0)$ and $v'(0)$ using (46) and (47), substituting into (48) and (49) and solving for u(0) and v(0), yields,

$$u(0) = h_u U/[h_u + D_u B_u \tanh(B_u L)] \qquad (50)$$

$$v(0) = V + [u(0)D_v/h_v](B_v^2/B_u) \tanh(B_u L) \qquad (51)$$

Thus, the H_2O and H_2 profiles in a finite slab for H_2O oxidation are given by (46) and (47), with the surface concentrations given by (50) and (51).

At low partial pressures, $P_{H2O} < 300$ Pa, this sequential method overestimates both the H_2O and H_2 concentrations: H_2O because H_2 inhibition is not accounted for, and H_2 because its source, the oxidation rate, is overestimated. However, it provides a view of H_2O and H_2 distributions in graphite fairly easily. However, the sequential estimates should be fairly accurate for high H_2O pressures ($P_{H2O} > 300$Pa) where Burnette's constants predict small effect of H_2 inhibition.

Figures 11, 12, and 13 show H_2O and H_2 profiles in a slab of 1-cm half thickness for temperatures of 900, 1100, and 1300 K. Oxidation parameters reported by Burnette et al (1978) for H451 graphite were use in the estimates. Free stream concentrations of 300 Pa H_2O and zero Pa H_2 were assumed.

Fig. 11 PH2O, PH2 vs. Depth
T = 900 K, PH2O = 300 Pa, PH2 = 0
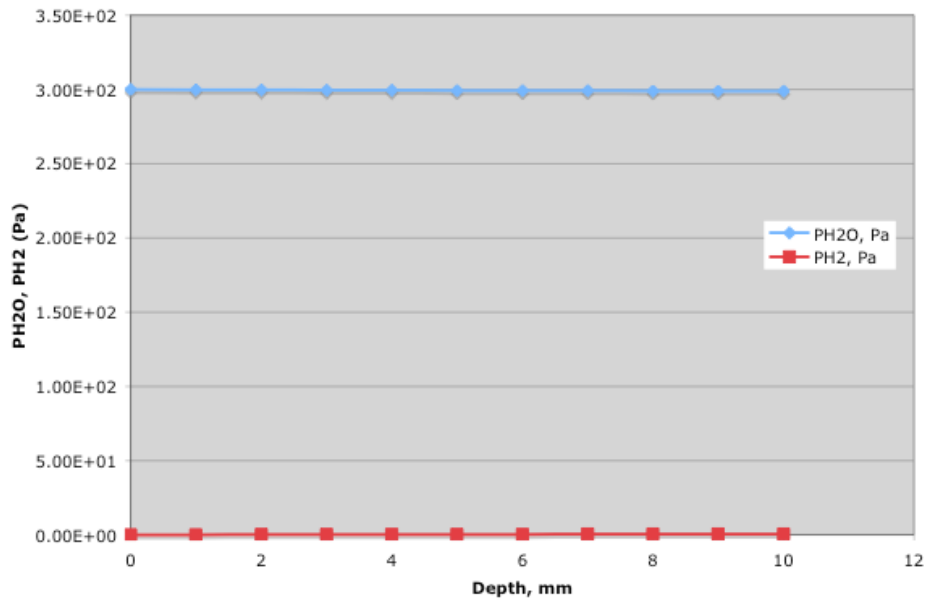Deff = 1%D Hndbk

Fig. 12 H2O and H2 Distribution in Slab
T = 1100 K, PH2O = 300 Pa, PH2 = 0
Deff = 1% D Hndbk
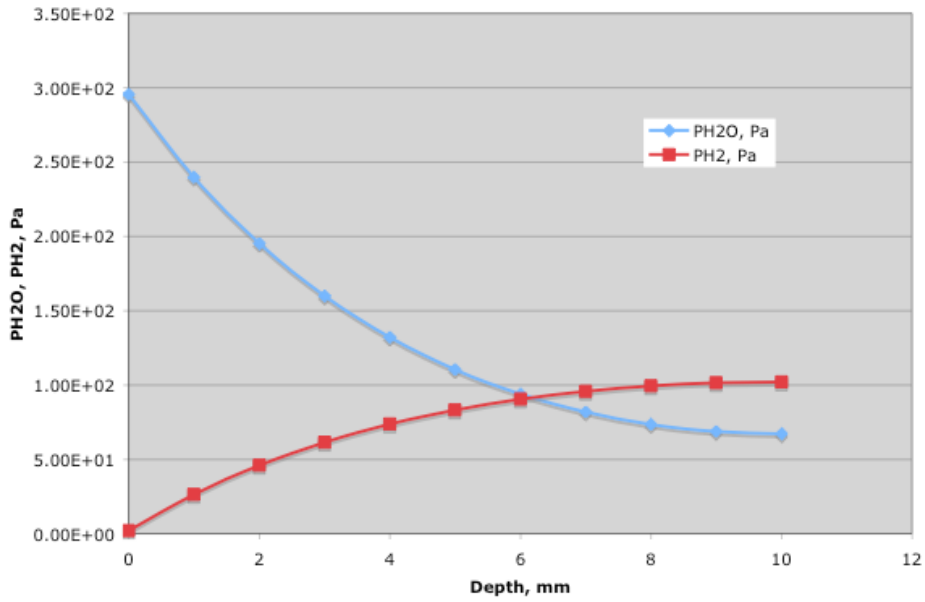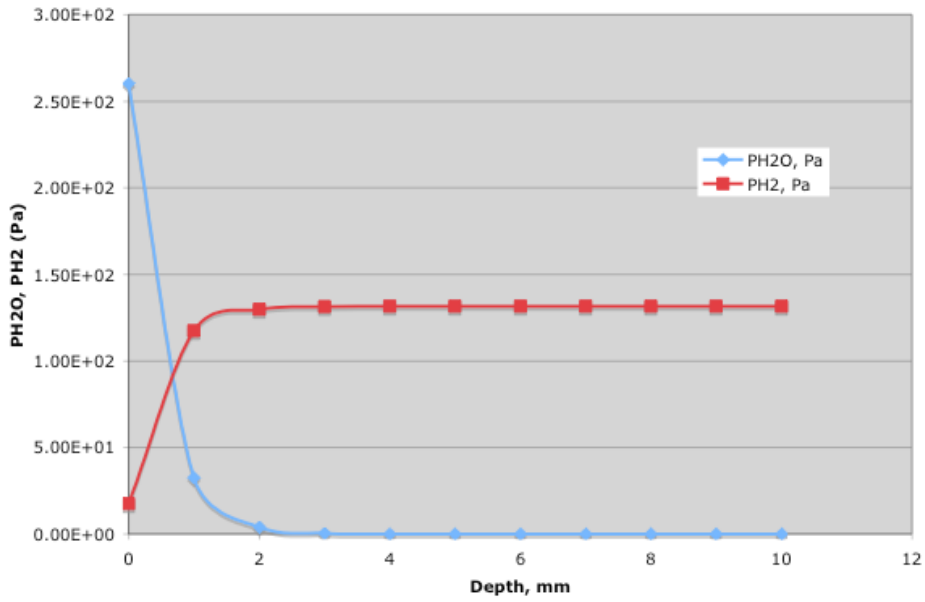**e-Folding Depth = 4 mm**

Fig. 13 PH2O, PH2 vs. Depth
T = 1300 K, PH2O = 300 Pa, PH2 = 0 Pa
Deff = 1%D Hndbk

At 900 K (Fig. 11), the oxidation rate is quite low, such that the free stream concentrations of 300 Pa H_2O and 0 Pa of H_2 are maintained throughout the sample. An ideal situation for a zone-1 sample test is predicted.

At 1100 K (Fig. 12), a significant drop is predicted in H_2O level to about 60 Pa at mid-plane. The H_2 level is seen to build to about 100 Pa, compared with 0 Pa in the free stream. Note that H_2 removal from the graphite by diffusion requires a consistent positive concentration slope from the surface to the mid-plane.

At 1300 K (Fig. 13) H_2O is completely exhausted at about 2 mm from the surface, at which point the H_2 level reaches about 140 Pa, and remains constant to the mid-plane. The "active oxidation depth", terminology used in GRSAC[6] (Wichner and Ball, 1999) of 2 mm at 1300 K is consistent with predictions used in GRSAC, as seen from Fig. A.2 in the reference. (It's actually about 1.5 mm in the cited reference.)

Note also that the surface concentration of H_2O at 1300 K is predicted to fall to 260 Pa, down from the 300 Pa value in the free stream. This is due to the higher demand for H_2O in the more reactive graphite requiring a 40 Pa concentration driving force in the free stream to deliver H_2O to the surface.

---

[6] Graphite Reactor Severe Accident Code

10. WATER AND HYDROGEN CONCENTRATION PROFILES IN A CYLINDER

10.1 Water Transport in Long Cylinders

Analogous to above treatments, the quasi-steady H_2O transport equation for a long cylinder, assuming linearized oxidation kinetics may be written,

$$0 = D_u[(1/r)\ d/dr(r\ du/dr)] - A_u\ u \tag{52a}$$

Or, in more convenient format,

$$0 = (1/r)\ d/dr(r\ du/dr) - B_u^2 u \tag{52b}$$

The solution of (52b) is identical to that given above for O_2 in cylinders, except that it is necessary to distinguish between H_2O and H_2 parameters. For H_2O parameters in (52),

u H_2O concentration in the graphite, mol/m_3-void
D_u effective diffusivity of H_2O
A_u $K_1 \cdot exp(-H/RT) \cdot RT \cdot \rho \cdot N_{H2O}$
B_u^2 A_u/D_u
N_{H2O} stoichiometric constant, mol H_2O reacted/mol C oxidized

H_2 parameters will be identified by the subscript v. Equation (52) is the zero order Bessel equation with solution,

$$u(r) = C_1\ I_0(B_u r) + C_2\ K_0(B_u r) \tag{53}$$

I_0 and K_0 are the zero order, modified Bessel functions of the first and second kind, respectively. Since K_0 goes to infinity as $r \rightarrow 0$, C_2 must equal zero. And since $I_0 = 1$ at $r = 0$, C_1 is identified as $u(0)$, the H_2O concentration at the center of the cylinder. Therefore, the solution for the H_2O concentration becomes

$$u(r) = u(0)\ I_0(B_u r) \tag{54}$$

Setting $r = a$, the cylinder surface, the H_2O concentration in the graphite at the surface, $u(a)$, is

$$u(a) = u(0)\ I_0(B_u a).$$

Substituting into (54) leads to,

$$u(r) = u(a)\ I_0(B_u r)/I_0(B_u a). \tag{55}$$

The surface concentration, $u(a)$, is determined from the free stream concentration of H_2O, the surface mass transfer coefficient, and the rate of diffusion from the surface. As already determined for O_2 (32),

$$u(a) = h_u U/[h_m + D_u\ B_u\ I_1(B_u a)/I_0(B_u a)] \tag{56}$$

Thus the H_2O concentration in the cylinder is given by (55), with the surface concentration given by (56).

10.2 Hydrogen Concentrations in a Cylinder

Analogous to the treatment for the finite slab, the H_2 source is directly related to the local oxidation rate, $A_u \cdot u$, except using the stoichiometric constant N_{H2} instead of N_{H2O}. Therefore the quasi-steady H_2 transport equation for the long cylinder may be written

$$0 = D_v(1/r) \, d/dr(r \, dv/dr) + A_v \, u \qquad (57a)$$

Or, more conveniently,

$$0 = (1/r) \, d/dr(r \, dv/dr) + B_v^2 \, u \qquad (57b)$$

where,

v local concentration of H_2
D_v effective diffusivity of H_2
A_v $K_1 \exp(-H/RT) \, RT \, r \, N_{H2}$
B_v^2 A_v/D_v
N_{H2} stoichiometric constant, mol H_2 produced/mol C oxidized

Recasting (57b), using the results for the H_2O distribution,

$$(1/r) \, d/dr(r \, dv/dr) = -B_v^2 \, u(a) \, I_0(B_u r)/I_0(B_u R) \qquad (58)$$

Integrating (58) once, using the symmetry about $r = 0$ leads to,

$$dv/dr = -[B_v^2 \, u(a)/I_0(B_u a) \, B_u] \, I_1(B_u r)$$

A second integration leads to,

$$v(r) = v(a) + (B_v/B_u)^2 \cdot u(r)[1 - I_0(B_u r)/I_0(B_u a)]. \qquad (59)$$

$v(a)$, the H_2 concentration in the graphite at the surface is obtained from, V, the free stream concentration of H_2 and h_v, the mass transfer coefficient for H_2. Noting that H_2 mass transfer is always in the direction graphite to free stream,

$$h_v \, (v(0) - V) = -D_v(dv/dr) \text{ at } r = a. \qquad (60)$$

Since mass transfer coefficient in the laminar regime is proportional to the diffusivity, h_v will be significantly higher than h_u. Evaluating the derivative using (59) and solving for $v(a)$ yields,

$$v(a) = V + \left[\frac{D_v}{h_v}\right]\left[\frac{B_v^2}{B_u}\right]u(a)\frac{I_1(B_v a)}{I_0(B_v a)} \qquad (61)$$

Thus the H_2 concentration in the graphite cylinder is given by (59), with the surface concentration, $v(a)$, given by (61).

Portrayal of these profiles generally shows similar dependency with temperature as already seen for the slab.

10.3 Surface Oxidation of a Long Cylinder

The surface oxidation rate, R_3 moles C oxidized per meter length per second, is obtained by integrating the following from $r = 0$ to the outer radius, a.

$$R_3 = \int_o^a R_1(r)\ r\ 2\pi r\ dr \tag{62}$$

As before, R_1 is the diffusion-unaffected rate. For linearized kinetics R_1 is given by,

$$R_1(r) = K_1 \bullet \exp(-H/RT)\ RT\ u(r) \tag{63}$$

Substitution of (63) into (62), using (56) for u(r) yields for the surface rate

$$R_3 = 2\pi K_1 \exp\left[-\frac{H}{RT}\right]\rho RT \frac{au(a)}{B_u}\left[\frac{I_1(B_u a)}{I_0(B_u a)}\right] \tag{64}$$

10.4 Zone-1 Criterion for a Long Cylinder

The oxidation efficiency, η, for H_2O is the same as derived for O_2, given by (36), except that that the constant, B, is specified for H_2O; therefore, for H_2O oxidation of a cylinder,

$$\eta = \frac{2}{aB_u}\left[\frac{I_1(B_u a)}{I_0(B_u a)}\right] \tag{65}$$

Figure 14 shows the variation of η with temperature determined from (65) for H_2O oxidation of a 1-cm radius cylinder of H451. D_{eff} has been assumed to be 0.01 D_{gas}. The figure shows that near zone-1 conditions ($h > 0.8$) would be maintained for this sample up about 1050 K.

A similar curve for O_2 oxidation of a typical structural graphite is co-plotted, using the same assumption regarding D_{eff}. As expected, zone-1 conditions ($\eta > 0.8$) end at a much lower temperature, about 850 K instead of 1050, due to the higher reactivity of O_2 relative to H_2O.

Fig. 14 Oxidation Efficiency vs. Temperature
1-cm Radius Cylinder, H2O and O2 Oxidation
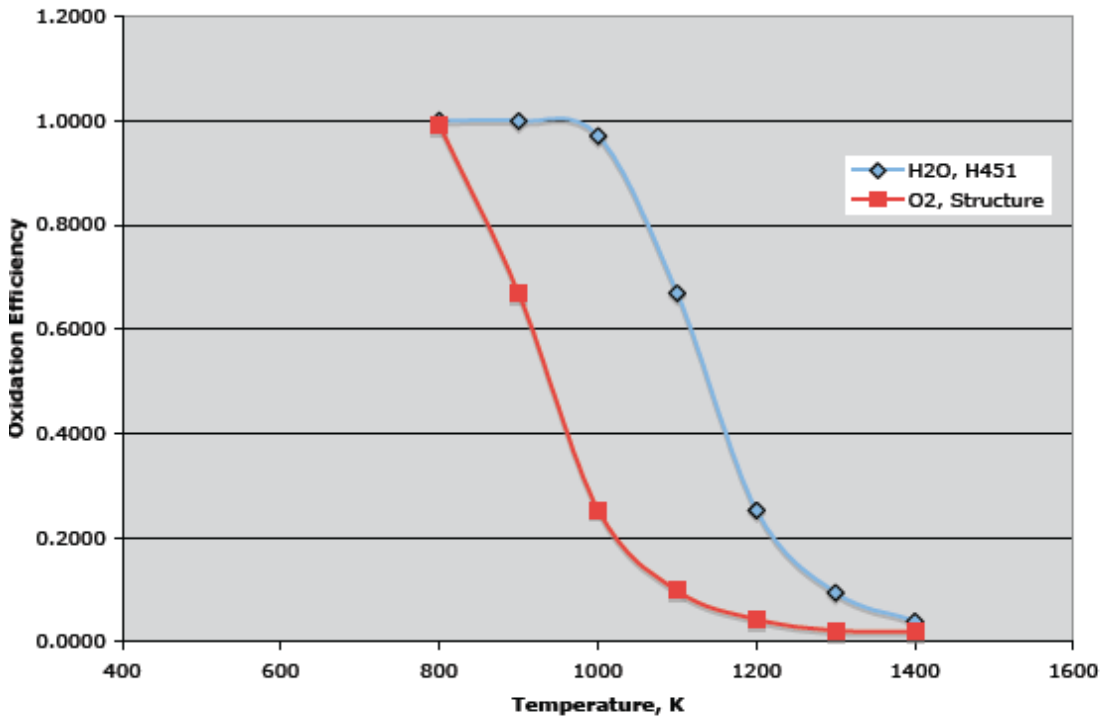
11. CONCLUSIONS

The density at any location and time in an oxidizing graphite member may be determined from Equation (1) provided the chemical rate, determined from the zone-1 kinetics equation, is known at each location and for all times. This requires full description of the oxidant distribution (and H_2 distribution for H_2O oxidation). Thus determination of impurity transport in graphite is key to solution of the general oxidation equation.

The spreading rate of oxidant (and H_2) in graphite is best described in terms of a Fickian expression using an effective diffusivity. The concept is most appropriate at the low impurity concentrations expected for normal operation. An idealized derivation indicates that in such case D_{eff} would equal the product of a pore configuration term and the handbook value of diffusivity in the gas mixture. At low burnoffs, the configuration factor was measured to be about 0.01 for British nuclear graphites.

The effective diffusivity method is not a good fit at higher impurity concentrations typical for air oxidation. In such case, diffusion–induced convection additionally contributes to the transport. However, there does not appear to be a reasonable alternative to use of an effective diffusivity. Very likely, proper evaluation of D_{eff} would be more difficult, with possibly an oxidation-rate sensitivity.

Linear approximations of the oxidation kinetics equation and assumption of constant effective diffusivity enable ready solution of quasi-steady state distribution of oxidant (and H_2 for the case of oxidation by H_2O) in regular geometries. The concentration profiles may be translated into

43

graphite density profiles. Coupling with surface convection enables visualization of surface effects.

Oxidant concentration profiles may be integrated to determine the surface oxidation rate, which may then be used to develop an "oxidation efficiency" parameter. Expressions are given for the finite slab and long cylinder. The parameter is useful for assessing zone-1 conditions for laboratory tests.

It is shown by more complete derivation, that the apparent activation energy of the surface oxidation rate of a semi-infinite slab approaches the traditional value of one half the zone-1 value at high temperature. The apparent activation energy may also be influenced by surface convection limitations.

Accuracy limitations of the illustrated methods result from assumption of constant effective diffusivity and linearization of the kinetics equation. Errors caused by assumption of constant Deff may be minimized by restricting estimates to low burnoff. Linearization errors may be reduced by re-optimizing kinetics constants for the assumed linear dependency. Despite these limitations, the simplicity of the methods are nevertheless useful for scoping estimates.

The additional limitation of an assumed quasi-steady state is not restrictive due to a predicted rapid approach to equilibrium above about 800 K.

NOMENCLATURE

a cylinder radius, m

A parameter in the O_2 transport equations, m^3-void/m^3-geom•sec

A_u, A_v similar parameters for H_2O and H_2, respectively

B parameter in O_2 transport equations, 1/m-geom

B_u, B_v similar parameters for H_2O and H_2, respectively

BO fractional burnoff

D_{gas} handbook value of gas diffusivity, m^2/sec

D_{eff} effective diffusivity of O_2 in graphite

D_u, D_v effective diffusivities of H_2O and H_2 in graphite

$f(\alpha)$ oxidation conversion function

h_m mass transfer coefficient for O_2, m/sec

h_u, h_v mass transfer coefficients for H_2O and H_2

J molar flux, mol/m^2-geom•sec

K_1 kinetics constant, mol C oxidized/mol C•sec•Pa

K_2, K_3 kinetic constants in H_2O oxidation equation, 1/Pa

L half-width of slab, m

m semi-empirical constant relating D_{gas} to D_{eff}

N_{H2} moles of H_2 produced per mole C oxidized

N_{H2O} moles of H_2O reacted per mole C oxidized

N_{O2} moles of O_2 reacted per mole C oxidized

n reaction order

P_{O2} partial pressure O_2, Pa

R_1 chemically controlled oxidation rate, mol C oxidized/mol C•sec

R_3 surface oxidation rate, mol C oxidized/m^2•sec for the slab, mol C oxidized/length•sec for the cylinder

u concentration of oxidant in graphite, mol/m^3-void

v concentration of H$_2$ in graphite, mol/m^3-void

α fractional oxidation, Eq. (5)

ε void fraction, m^3-void/m^3-geom

η oxidation efficiency for slab, Zone-1 criterion   parameter

η oxidation efficiency cylinder,

ρ graphite molar density, mol C/m^3-geom

ρ_∞ unoxidized molar density of graphite, mol/m^3

ρ_{theo} theoretical graphite molar density, mol/m^3

REFERENCES

Aris, R. (1975), <u>The Mathematical Theory of Diffusion and Reaction in Permeable Catalysts, Vol. I The Theory of the Steady State</u>, Clarendon Press, 1975

Burnette, R.D., et al (1978), "Oxidation of H451 Graphite by Steam", GA-A-14951, Aug. 1978

Carlslaw, H.S. and J.C. Jaeger (1956), <u>Conduction of Heat in Solids</u>, Oxford Clarendon Press, 2nd Ed.

Contescu, C.I. et al, (2008), "Practical aspects for Characterizing Air Oxidation of Graphite", J. Nucl. Mater., 381: 15-24.

Coulson, J.M. and J.F. Richardson (1991), <u>Chemical Engineering</u>, Vol. 3, p. 119, Pergamon Press

Evans, R.B., G.M. Watson, and E.A. Mason (1961), "Gaseous Diffusion in Porous Media at Uniform Pressure", J. Chem. Phys, vol. 33, 2076

GDH (1988), "Graphite Design Handbook", Issued by General Atomics, DOE-HTGR-88111, Sept. 1988

Hawtin, et al (1964), "The Effect of Diffusion and Bulk Gas Flow on the Thermal Oxidation of Nuclear Graphite – I Temperatures Below 500°C", Carbon, 2: 299-301.

Hawtin, P, and J.A. Gibson (1966), "The Effect of Diffusion and Bulk Gas Flow on the Thermal Oxidation of Porous Carbons – II Diffusional Effects in Graphite at High Temperatures", Carbon, 4: 489-500

Hawtin, P, J.A. Gibson, and R.A. Huber (1967), "Air Oxidation Studies in a Long Graphite Channel", Carbon, 6: 901-915.

HC&P (2004), <u>Handbook of Chemistry and Physics</u>, 85th Edition, CRC Press

Hewitt, G.F. and J.R. Morgan (1961), "The Diffusion of Oxygen in Nitrogen in the Pores of Graphite", AERE-R- 3814, 1961

Hines, A.L. and R.N. Maddox, <u>Mass Transfer</u>, Prentice-Hall, 1985

Hinssen, H-K, et al (2006), "Oxidation Experiments and Theoretical Examinations on Graphite Materials Relevant for the PBMR", Proceeding HTR2006, Oct 1-4 2006, Johannesburg, SA, pp. 1-10

Katscher, W. (1988), "Dichteanderung von Reaktorgraphiten als Folge der Graphit/Sauerstoff-Reaktion im Porendiffusionsbereich" Unpublished KfA Report

Petersen, E.E. (1965), "A General Criterion for Diffusion Influenced Chemical Reactions in Porous Media", Chem. Eng. Sci., 20: 587-591.

Ruthven, D.M. (1983), <u>Principles of Adsorption and Adsorption Processes</u>, John Wiley and Sons

Weisz, P.B. and C.D. Prater (1954), "Interpretation of Measurements in Experimental Catalysis", Advances in Catalysis, 6: 167.

Wichner, R.P. and S.J. Ball (1999), "Potential Damage to Gas-Cooled Reactors Due to Severe Accidents", ORNL/TM-13661, April, 1999

APPENDIX A: EQUILIBRATION TIMES FOR DEVELOPMENT OF THE QUASI-STEADY PROFILES

Consider the following equation for transient diffusion in a slab,

$$\partial u / \partial t = Cu'' - Du ,$$

(A.1)

with boundary conditions,

BC1: $u(x) = 0$ at $t = 0$ for all x,
BC2: $u(0) = U$ for all following times.

Comparing (A.1) with the transient oxidant transport equation (2), we identify

$$C = D_{eff} / \varepsilon$$
$$D = A / \varepsilon .$$

Consistent with treatments in this memo, the void fraction, ε, and D_{eff} have been assumed constant. Carslaw and Jaeger (1959, Section 4.2) give the solution of (A.1) in terms of oxidation parameters,

$$\frac{u(x,t)}{U} = 0.5 \exp\left[-x\sqrt{\frac{A}{D_{eff}}} \right] erfc(\text{arg}1) + 0.5 \exp\left[x\sqrt{\frac{A}{D_{eff}}} \right] erfc(\text{arg}2)$$

(A.2)

where,

$$\text{arg}1 = \frac{x}{2\sqrt{\frac{D_{eff}t}{\varepsilon}}} - \sqrt{\frac{At}{\varepsilon}}$$

$$\text{arg}2 = \frac{x}{2\sqrt{\frac{D_{eff}t}{\varepsilon}}} + \sqrt{\frac{At}{\varepsilon}}$$

The complementary error function, erfc(z), has a maximum value of 2 at $z = -\infty$ and rapidly declines with increasing z. It is essentially zero for $z > 3$. At small t, $arg1$ and $arg2$ take large positive values, thus the erfc functions are near zero, satisfying BC1. At large t, (A.2) shows that $u(x,t) = U$ at $x = 0$, satisfying BC2. Also note that at large t, erfc($arg1$) approaches 2 and erfc($arg2$) approaches o. Thus (A.2) tends to the exponential profile predicted for the time-steady case for a semi-infinite slab.

Examination of (A.2) shows that the equilibrium profile is approached asymptotically. Therefore $u(x,t)$ at the equilibrium time is not a true extremum, and hence cannot be determined explicitly by setting the time derivative of $u(x,t)$ equal to zero. Moreover, the approach to equilibrium proceeds at different rates at different locations; surface locations equilibrating more rapidly than the interior.

The most direct method for determining the equilibration time, though limited in scope, is to simply observe the profiles plotted from (A.2) for a series of increasing times. Using preliminary kinetics parameters for O_2 oxidation of a structural graphite and evaluating D_{eff} for O_2 in He, yields the O_2 profiles shown in Fig. A.1 and A.2. Figure A.1 for 800 K shows that 200 seconds is a close approximation of the time required to equilibrate, at least up to an 80cm depth. Figure A.2 for 1000 K indicates an equilibration time of about 10 seconds, again up to an 80-cm depth. A similar profile for 1200 K shows an equilibration time of <1 second. Results are summarized in Table A.1.

Table A.1 Equilibration Times for O_2 Oxidation of a Structural Graphite

Temperature, K	Equilibration Time, sec
800	200
1000	10
1200	<1

Equilibration times for H_2O oxidation are expected to be significantly longer due to the lower oxidations rate, hence greater oxidation depth.

Fig. A.1 Transient O2 Profiles, 800 K
Structural Graphite
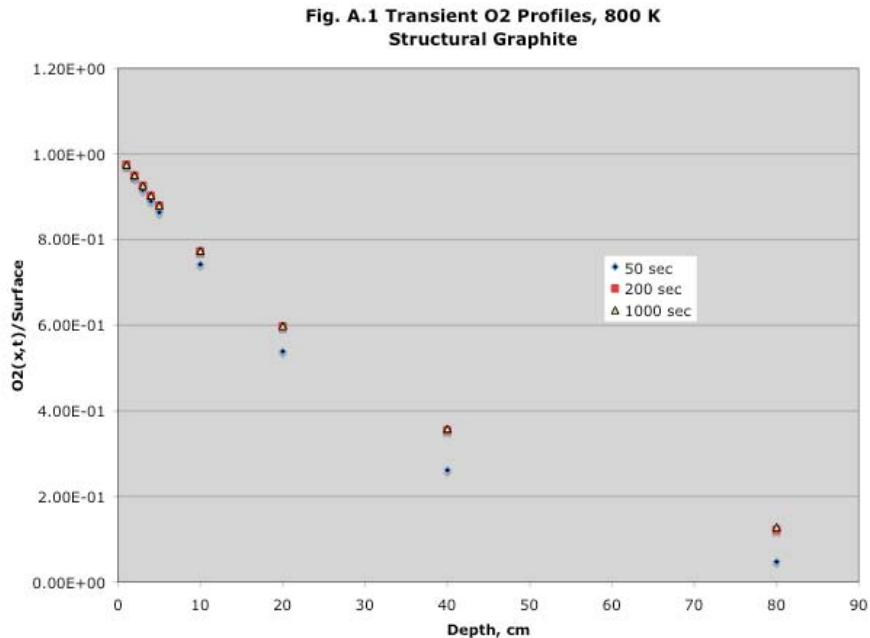
Fig. A.2 Transient O2 Concentration Profiles, 1000 K
Structural Graphite